


1997

Development of a pulsed eddy current instrument and its application to detect deeply buried corrosion

William Westfall Ward III
Iowa State University

Follow this and additional works at: <https://lib.dr.iastate.edu/rtd>

 Part of the [Other Materials Science and Engineering Commons](#), and the [Signal Processing Commons](#)

Recommended Citation

Ward, William Westfall III, "Development of a pulsed eddy current instrument and its application to detect deeply buried corrosion" (1997). *Retrospective Theses and Dissertations*. 16795.
<https://lib.dr.iastate.edu/rtd/16795>

This Thesis is brought to you for free and open access by the Iowa State University Capstones, Theses and Dissertations at Iowa State University Digital Repository. It has been accepted for inclusion in Retrospective Theses and Dissertations by an authorized administrator of Iowa State University Digital Repository. For more information, please contact digirep@iastate.edu.

Development of a pulsed eddy current instrument and its application to detect
deeply buried corrosion

by

William Westfall Ward III

A thesis submitted to the graduate faculty
in partial fulfillment of the requirements for the degree of
MASTER OF SCIENCE

Major: Electrical Engineering

Major Professor: Satish Udpa

Iowa State University

Ames, Iowa

1997

Copyright © William Westfall Ward III, 1997. All right reserved.

Graduate College
Iowa State University

This is to certify that the Master's thesis of

William Westfall Ward III

has met the thesis requirements of Iowa State University

Signatures have been redacted for privacy

TABLE OF CONTENTS

LIST OF FIGURES	vi
CHAPTER 1. INTRODUCTION	1
1.1. Problem Definition.....	1
1.2. Scope of Thesis	2
1.3. Background	4
1.3.1. Nondestructive Evaluation	4
1.3.2. Eddy Currents in NDE	6
1.3.3 Pulsed Eddy Currents	8
CHAPTER 2. SYSTEM DESIGN.....	10
2.1. Description	10
2.2. Probe Design	10
2.2.1. Coil Sensor: Absolute Mode	10
2.2.2. Coil Sensor: Reflection Mode	13
2.2.3. Magnetic Sensor	14
2.3. PEC Board.....	14
2.4. Analog-to-Digital Converter	17
2.5. Scanner, Stepper Motors, and Controller Board	17
2.6. Personal Computer and Software	17
2.7. Constant Current Drive	19
2.8. Magnetic Sensor Circuitry.....	21

CHAPTER 3. COIL SENSOR: ABSOLUTE MODE	22
3.1. Description	22
3.2. Theory	22
3.3. Experimental Setup	26
3.4. Results	26
3.5. Conclusions	31
CHAPTER 4. MAGNETIC SENSORS FOR DEEP PENETRATION	33
4.1. Description	33
4.2. Motivation	33
4.3. Theoretical Results	35
4.4. Giant Magnetoresistive Sensors	36
4.4.1. Description	36
4.4.2. Comparison to other sensors	39
4.5. Experimental Results	40
4.5.1. Experimental Setup	40
4.5.1.1. Electronics	40
4.5.1.2. Probe Design	40
4.5.1.3. Test Sample	42
4.5.2. Experimental Results	43
4.6. Conclusions	48
CHAPTER 5. CONCLUSIONS	49
5.1. Summary	49

5.2. Future Work 50

APPENDIX A. CODE FOR ABSOLUTE COIL SENSOR THEORY 52

**APPENDIX B. PUBLISHED PAPER: “LOW FREQUENCY, PULSED
EDDY CURRENTS FOR DEEP PENETERATION” 58**

BIBLIOGRAPHY 67

LIST OF FIGURES

Figure 2.1. Block diagram of pulsed eddy current instrument.....	11
Figure 2.2. Block diagram of the absolute mode of operation.....	12
Figure 2.3. Block diagram of the reflection mode of operation.....	13
Figure 2.4. Block diagram of magnetic sensor configuration using a giant magnetoresistive bridge sensor.....	15
Figure 2.5. Block diagram of pulsed eddy current electronic hardware.....	17
Figure 2.6. Schematic diagram of constant current drive.....	20
Figure 3.1. Schematic of the coil used for theoretical modeling.....	24
Figure 3.2. Samples using 2024 Aluminum plates	27
Figure 3.3. Characteristic pulsed eddy current signal	28
Figure 3.4. Comparison of theory and experiment for increasing amounts of corrosion located on the bottom of the top plate	29
Figure 3.5. Comparison of theory and experiment for increasing amounts of corrosion located on the top of the bottom plate	30
Figure 3.6. Comparison of theory and experiment for increasing amounts of corrosion located on the bottom of the bottom plate	31
Figure 4.1. Theoretical predictions of the coil sensor and GMR sensor for detecting 10% corrosion on the bottom of a 2024 Al panel	37
Figure 4.2. Schematic of the GMR sensor	38
Figure 4.3. Design of GMR sensor electronics	41
Figure 4.4. GMR probe design for the pulsed eddy-current system.....	42
Figure 4.5. The 6.35 mm thick sample with flat bottom holes on the bottom of the plate to simulate corrosion.....	43

Figure 4.6. The 12.7 mm thick sample is made up of two 6.35 mm plates with flat bottom holes on the bottom of the sample to simulate corrosion..... 43

Figure 4.7. Signals for simulated corrosion on the bottom of a 0.250” panel of 2024 Al 45

Figure 4.8. Scanned images using the GMR probe to detect simulated corrosion on the bottom a 0.250” thick panel of 2024 Al..... 46

Figure 4.9. Signals for simulated corrosion on the bottom of a 0.500” panel of 2024 Al 47

CHAPTER 1. INTRODUCTION

1.1. Problem Definition

Many industries in our society depend on the use of machines for almost every task imaginable. Over time these machines will begin to degrade with age and fatigue to the point that they may fail in a catastrophic way. In certain applications a failure of this type is unacceptable because of the probability of resulting personal injury or loss of life. One way to prevent this is to anticipate where the weak point will be and estimate the earliest time at which the part may fail and then replace all the affected parts before they fail. However, the majority of the parts may have only a small portion of their life used when they are replaced and have many more years of useful life. Thus this method is very expensive and inefficient to implement. It is obvious that if only the parts which needed to be replaced because they were nearing the end of their lifetime were replaced, a great savings would be realized and would not degrade the safety of the machine.

The purpose of nondestructive testing is to do just that: identify when a part is near failure without damaging the part in the process of testing. Two large industries which use nondestructive evaluation to inspect their equipment are the aircraft industry and the nuclear power generation industry. Aircraft have problems with fatigue cracking and corrosion over time. In aircraft turbine engines, cracks can also develop and, if not detected in time, can cause the engine to catastrophically fail in flight. Problems with corrosion are also present in the skin of many aircraft. The lap joints are particularly susceptible to corrosion when water seeps into the joints and causes the aluminum skin to corrode from the inside, where it cannot be seen. In the nuclear industry, the heat exchanger tubes are a barrier that isolates

radioactive cooling water in the reactor from the outside environment. These tubes are susceptible to cracking and, if a crack is not detected in time, a radiation leak can develop.

The problems mentioned above are very difficult, if not impossible, to detect by the naked eye because of inaccessibility. Either the inspector cannot get in a position to see the part where problems develop or the problem is hidden from view, such as in the case of a lap joint. Thus there is a need for instruments that can detect the flaws which cannot be seen.

This thesis will discuss two variations of the pulsed eddy current method of nondestructive evaluation to detect corrosion. The constant current drive that is discussed in Chapter 3 has been used to detect corrosion in aircraft skin and can effectively detect corrosion and discriminate which layer of metal is corroded. The second variation, use of magnetic sensors for pulsed eddy current, which is discussed in Chapter 4, is for the purpose of detecting corrosion in thick plates of material. This may be useful for detecting corrosion problems in structural members of aircraft or may be extended in the future to detect cracks buried under thick layers.

1.2. Scope of Thesis

The remainder of this chapter briefly describes the field of nondestructive testing and then reviews the background of eddy current testing, summarizing some of the benefits and shortcomings of various techniques. Following this, there is an introduction to the techniques which are used in eddy current testing.

Chapter 2 focuses on the system that was designed for the pulsed eddy current instrument. The core of the system is a portable computer with a custom made pulsed eddy current expansion board, an analog-to-digital converter, and the scanner with controller

board. A custom designed WindowsTM software package allows the user to control the system and display and analyze results. Pulsed eddy current methods have been under development in the Center for NDE since 1991, under the direction of John Moulder. The pulsed eddy current expansion board was designed and built by the author. The software was created by Mark Kubovich, Sunil Shaligram, Jerry Patterson, and the author. Theoretical analysis of the system, based on Cheng, Dodd, and Deeds analysis, was developed by Erol Uzal and James H. Rose.

In Chapter 3, the pulsed eddy current system is extended to use a constant current drive source, which excites the coil with a step current instead of a step voltage to look for corrosion in a set of 1 mm thick 2024 aluminum plates, which model a lap joint in aircraft skin. The theoretical analysis is for layers of infinite length and width but can be used to approximate corrosion as long as corroded area is larger than the coil in the probe, since the eddy currents are somewhat localized under the coil. Next, experimental results are compared with the theory and are found to be in good agreement.

Then, in Chapter 4, the focus is on detecting corrosion deeply buried in the material. It is shown that a magnetic sensor has advantages over a coil sensor when penetrating to depths of several millimeters. This is due to the fact that the signal from the magnetic sensor does not fall off as quickly with depth of penetration as the coil because the coil responds to the time derivative of flux while the magnetic sensor responds to the magnitude of the magnetic field. An experiment is performed using 2024 aluminum plates, 6.35 mm and 12.7 mm thick, to compare the relative abilities of the coil and magnetic sensors to detect corrosion. For the magnetic sensor, a giant magnetoresistive bridge sensor was used for two

reasons. First, it is a small package for which it is easy to develop support electronics because it is driven as a typical bridge circuit with a bias current through the bridge and a differential output measured between the two legs of the bridge. Second, the technology is relatively new and it does not appear to have been applied to pulsed eddy currents to date. In this experiment, the predictions of the theory that the magnetic sensor would have a significantly stronger signal than the coil sensor were confirmed. When detecting corrosion on the bottom of a 12.7 mm thick plate, the magnetic sensor signal was nearly 8 times the strength of the coil sensor. Also, the magnetic sensor was able to detect as little as 2.5% corrosion on the bottom of the plate whereas the coil was only able to detect 10% corrosion at this depth. In this chapter, the author performed the circuit design, probe design, experimental work, and theoretical calculations. The theoretical modeling software was written by others, as cited in the chapter.

Finally, in Chapter 5, a number of conclusions about the work presented in this thesis are drawn and some ideas for future work are presented.

1.3. Background

1.3.1 Nondestructive Evaluation

There are many methods of testing available in the arena of nondestructive testing. Techniques such as magnetic particle and liquid penetrant are used to detect surface-breaking cracks by making the cracks more visible so that they can be seen by the human eye. Ultrasonic testing can also be used to detect surface flaws, to detect internal flaws, or for material thickness applications. However, it is limited to detecting through multiple layers only as deep as there is mechanical coupling between materials. For example, ultrasonic

inspection can look to the bottom of two plates of aluminum if the plates are pressed tightly together or there is a medium between the plates to allow the ultrasonic waves to propagate into the second layer of material. If there is an air gap between the two plates, the ultrasonic wave will not be able to propagate through the gap to the second plate. Radiographic inspection, X-ray inspection, is another method widely used in NDE. This requires a radiation source on one side of the test sample and a film or camera sensitive to the radiation on the other side. An image of the object under inspection is created on the detector, allowing for visual inspection of flaws at any location in the object. However its chief drawback for the applications listed above is that it requires access to both sides of the sample, which is often not available. It also entails use of hazardous radiation, which limits accessibility to the test object by other personnel.

The other common method of detection is eddy currents. This overcomes the coupling problem encountered in ultrasonic methods because a coupling medium is not required between the plates. Thus, it can be used on two layer structures that are separated by an air gap. Eddy currents, in their most common configurations at least, only require access to one side of the material being inspected, thus overcoming the limitation of X-rays. Eddy currents are, however, limited to conducting materials and typically do not have the same resolution as do ultrasonic and X-ray methods. X-ray also has the advantage of imaging an entire area almost instantaneously whereas eddy current and ultrasonic methods scan a point source over an area to create an image. Eddy currents are also limited by the skin depth effect which limits the depth of penetration of the eddy currents. This limits the thickness of material which can be inspected, especially in magnetic materials.

1.3.2 Eddy Currents in NDE

The heart of eddy current measurements is the probe. These come in a wide variety of configurations and sizes, but the fundamental principle of operation is the same for all. This discussion will focus on a probe with a single coil with a rectangular cross section.

The majority of eddy current instruments use a continuous sine wave of one fixed frequency as the drive for the eddy current coil. The probe is then placed on top of the material to be inspected. Since an alternating current is flowing in the coil, eddy currents are induced in the material. Due to the skin depth effect, the eddy current densities are strongest near the surface of the material and then decay exponentially as they penetrate deeper into the material. The skin depth is described as the point at which the current density has fallen off by e^{-1} and is dependent on the frequency of excitation and conductivity and permeability of the material, following the expression

$$\delta = \frac{1}{\sqrt{f\pi\mu\sigma}} \quad (1.1)$$

where δ is the skin depth, f is the frequency of excitation, μ is the permeability, and σ is the conductivity of the material. It can be seen that the depth of penetration of the eddy currents into the material is inversely proportional to square root of the frequency of excitation.

The flaws, whether they be corrosion or cracks, are detected by detecting the change in eddy currents. When a single coil sensor is used, a magnetic field is established by the current flowing through the drive coil. The eddy currents which are induced in the material create a magnetic field which is in opposition to the magnetic field established by the coil and lower in magnitude, thus changing the impedance of the coil compared to the impedance of

the coil in air. If a flaw is introduced in the path of the eddy currents, they must find a way to flow around the flaw since they cannot flow through a crack or corrosion. This will change the magnetic field created by the eddy currents and thus change the impedance of the coil. This change of coil impedance is monitored as the signal of interest. This description is relevant to a single coil method. Many different methods are in use, many of which use a differential probe consisting of two coils wound in opposition. These work in fundamentally the same way as the single coil method.

As a result of the skin depth effect, it can be inferred that if detectability of surface-breaking or near-surface flaws is desired, a relatively high frequency should be used and for flaws deeply buried in the material, a lower frequency should be used. However, with only one frequency of excitation, it is usually not possible to extract enough information to isolate a flaw in the material and determine the location in depth of the flaw as well as the size of the flaw. To allow for better interpretation of the results, some instruments, such as the MIZ-40, excite the coil at up to four frequencies to acquire more depth information to better characterize the flaw and eliminate unwanted effects such as probe lift-off.

The next advance is the swept frequency method. This method is the same as the fixed frequency except that the frequency is no longer fixed but swept over a range of frequencies producing eddy currents ranging from low frequencies, which penetrate deeply into the material, to the high frequencies which induce eddy currents near to the surface only. This results in more information which can be used to characterize the size and location of the flaw. However, this technique has the drawback that it is slow. Using the Hewlett Packard 4194A impedance analyzer for the measurement, a single point takes several

minutes, according to Moulder, et. al. [1]. This makes it undesirable for scanning applications simply because it is not fast enough.

1.3.3 Pulsed Eddy Currents

A faster method of acquiring data with a spectrum of frequencies is the pulsed eddy current method. This method uses a broadband pulse or step function to excite the coil and induce eddy currents in the material. The eddy currents that are induced then cover a range of depths and contain information equivalent to the swept frequency methods but only require milliseconds to acquire the data for a single point instead of minutes as with the swept frequency method.

Pulsed eddy currents have been receiving increasing interest recently. This, in large part, can be attributed to the advances in electronics in the past ten years. When the coil is excited with a step function, either a voltage or current response is recorded depending on whether the probe is excited with a current or voltage step. If the probe is excited with a voltage step, the current is measured to determine the impedance of the coil. If the probe is excited with a current step the voltage is measured to determine the impedance of the coil.

A signal over an area which does not have any flaws must first be recorded. This is called the null or reference signal and must somehow be subtracted from all subsequent signals to yield the change in impedance of the probe. For typical flaws, the magnitude of this change can be as small as one thousandth of the null signal, so some means of differencing is essential to viewing the signal. This null signal can be digitized by a high speed, high resolution analog-to-digital converter and stored in a portable computer. Subsequent traces can then be digitized in the same way and then subtracted digitally. Before

the technology was available to accomplish this easily, other methods had to be used to difference the response, such as using two identical coils. One coil would be placed on a reference standard to create the null signal and the second would be placed over the location to be inspected. The response of these two probes was then subtracted using analog signal processing and displayed on a oscilloscope. There are obvious disadvantages to this procedure. One is that a reference standard is required for every possible configuration of material to be measured. Also it is very difficult to create a null signal using the balancing coil and reference standard which do not vary by more that 0.1%. Also the advent of the personal computer makes it very easy to process the signal and display images. These two abilities in conjunction with each other make it much easier to scan a flaw quickly and accurately interpret the results.

CHAPTER 2. SYSTEM DESIGN

2.1. Description

The pulsed eddy current system consists of five components: (1) the probe, (2) the electronic hardware to drive the probe and condition the signal, (3) an analog-to-digital converter, (4) a scanner with associated motors and control circuitry, and (5) a personal computer with custom software that controls the entire system. A block diagram of the system is shown in Figure 2.1. The entire system is focused around a personal computer, which is portable and has five expansion slots. All of the electronics, with the exception of stepper motor power supplies, are contained in the PC as expansion boards, making the system portable and easy to set up. Each component of the system is discussed individually below.

2.2. Probe Design

There are three types of probes that have been used with this system. All three use a coil to create eddy currents in the material under test and are differentiated by the sensor used. The three types are absolute mode coil sensor, reflection mode coil sensor, and giant magnetoresistive sensor.

2.2.1. Coil Sensor: Absolute Mode

The absolute mode coil sensor uses the same coil to create the eddy currents in the material and to detect the signal from these eddy currents. Signals from this coil are derived from the change in impedance of the coil. The coil has an impedance in air that is primarily an inductive response due to the changing magnetic field which is created. When this coil is brought into the proximity of a conducting material, the coil will induce eddy currents in the

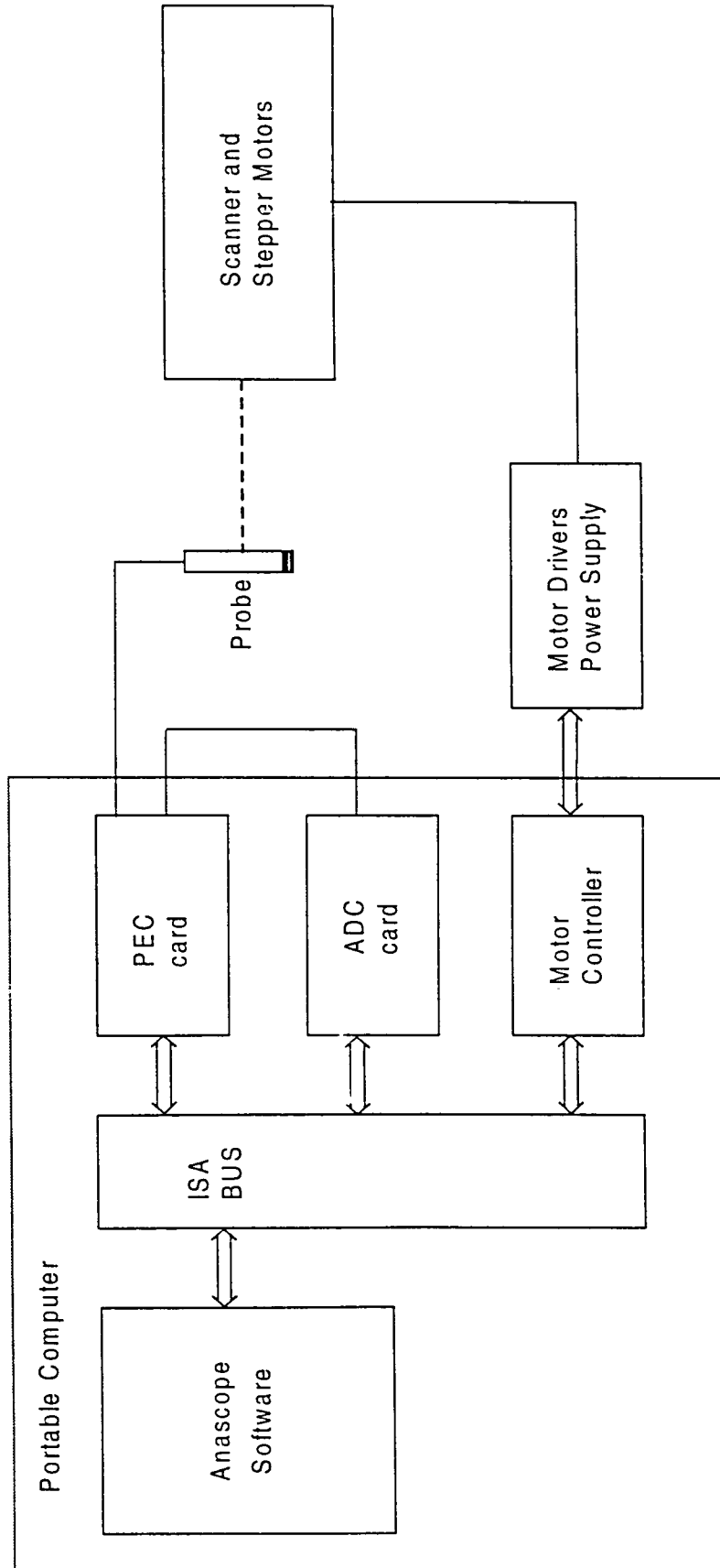


Figure 2.1. Block diagram of pulsed eddy current system.

material. These eddy currents will create a magnetic field that opposes the field set up by the current flowing in the coil. This changes the magnetic field that is threading the coil, thus changing the impedance of the coil.

The coil can be driven in two different ways: constant voltage or constant current. The constant voltage mode imposes a step voltage across the coil and the current through the coil is measured. Any changes in the material under test that change the flow of eddy currents created by the coil in the material will change the field created by the eddy currents, thus changing the impedance of the coil. This change in impedance can be observed as a change in current through the coil. This is pictured in Figure 2.2(a).

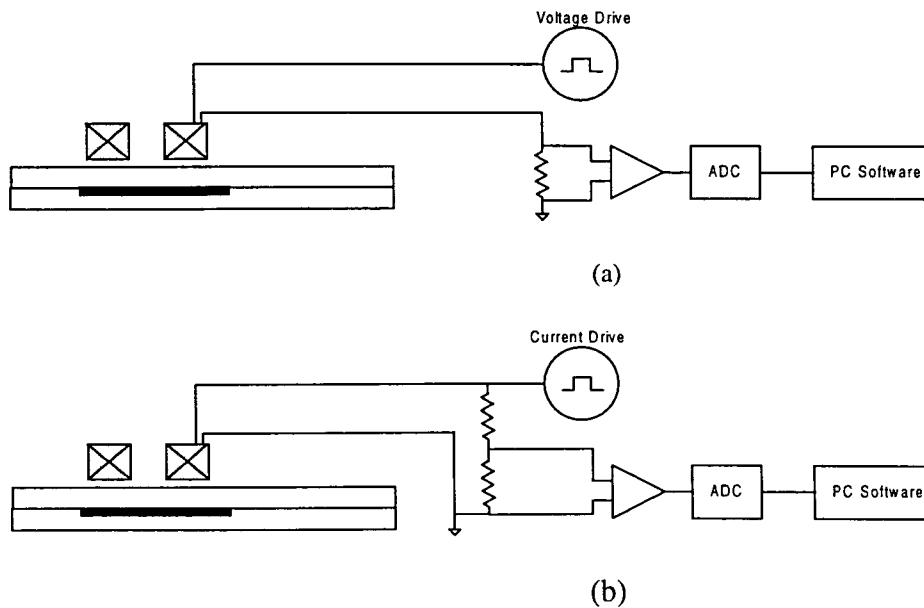


Figure 2.2. Block diagram of the absolute mode of operation using (a) constant voltage drive and (b) constant current drive.

The constant current mode imposes a step current across the coil and the voltage across the coil is measured. The step current, of course, has a finite rise time because the current through a perfect inductor cannot be changed instantaneously without an infinite voltage source. This will be discussed further under the design of the constant current drive in Section 2.7. As with the constant voltage mode of operation, a change in impedance is measured, except that when the current through the coil is controlled, the voltage across the coil must be measured through a voltage divider to determine the change in impedance. Refer to Figure 2.2 (b) for a schematic of this configuration.

2.2.2. Coil Sensor: Reflection Mode

The reflection mode is different from the absolute mode in that separate coils are used for the drive and receive functions, commonly called the transmit and receive coils, respectively. The drive coil can either be driven by a constant voltage or constant current drive waveform. The receive coil is usually smaller than the drive coil and is typically mounted coaxially so that the bottom of the receive coil is mounted flush with the bottom of the drive coil. Refer to Figure 2.3 for a schematic of this configuration.

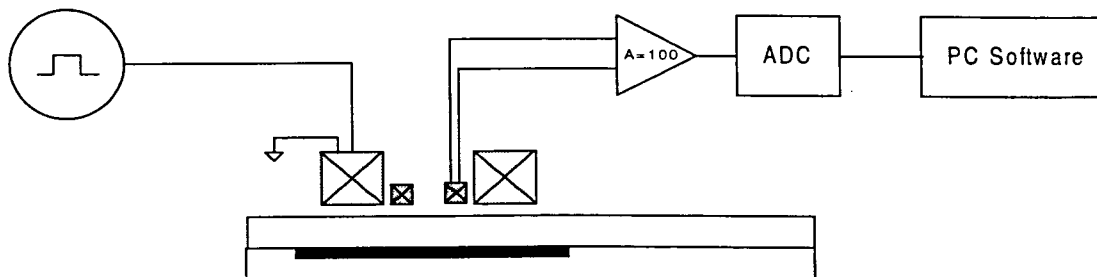


Figure 2.3. Block diagram of the reflection mode of operation.

In a reflection probe the drive coil generates the eddy currents in the material, as in the absolute mode. However, the signal of interest is the voltage induced in the receive coil. The voltage induced across the receive coil responds to the time derivative of the flux linking the coil. Thus, when the material changes due to the presence of a flaw in such a way that the eddy currents are changed, the portion of the flux linking the receive coil that is generated by the eddy currents is changed. Thus, a change in the voltage across the receive coil is observed.

2.2.3. Magnetic Sensor

This configuration performs in a similar manner to the reflection mode, except that a magnetic field sensor is used instead of a coil sensor. The magnetic sensor has an axis of sensitivity in one direction only, whereas the coil sensor responds to all of the magnetic flux that threads the coil. This axis of sensitivity is oriented along the axis of the drive coil and is centered in the coil. When the coil is driven by a constant current or a constant voltage, a magnetic field is created by the coil which will be detected by the magnetic sensor. When a conductive material is in proximity to the coil, eddy currents will be induced in the material, which will in turn create a magnetic field in opposition to that produced directly by the coil. When the flow of the eddy currents is interrupted by a change in the material, the magnetic field will change. This change can be directly detected by the magnetic sensor. Refer to Figure 2.4 for a schematic of this configuration.

2.3. PEC Board

The pulsed eddy current board was built by the author to perform pulsed eddy current measurements. It was designed to drive a coil in the constant voltage drive mode and can be

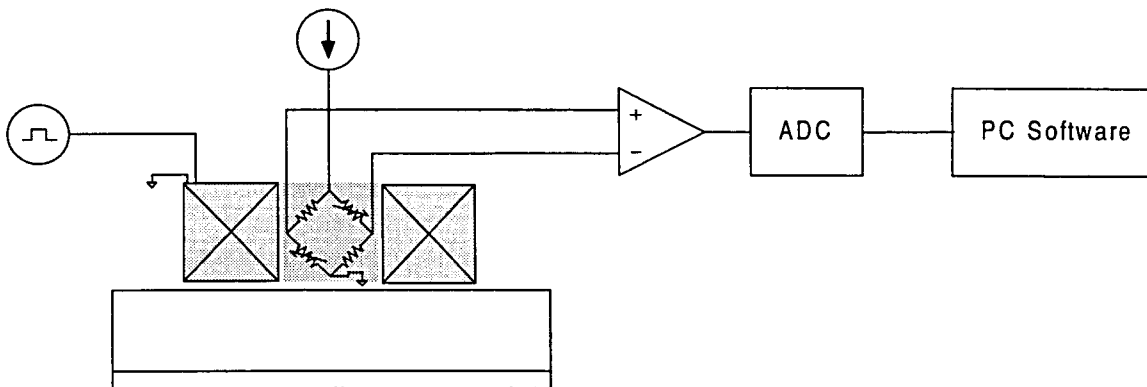


Figure 2.4. Block diagram of magnetic sensor configuration using a giant magnetoresistive bridge sensor.

operated in either absolute mode, where the drive coil is also the sense coil, or reflection mode, where a separate coil is used as the sense coil. It has been used as the basis for experiments performed at the Center for NDE for the last two years and is the basis for the experiments reported in several papers. [2-6]

The custom designed board interfaces with a PC via an 8-bit ISA bus. Please refer to Figure 2.5 for a block diagram. The card consists of circuitry to drive the probe in constant voltage mode and amplify the signal in both absolute and reflection modes. A microcontroller is also on the card to communicate with the personal computer and control the card.

The drive waveform is created as follows. A digital-to-analog converter is set to a value between zero and ten volts. This voltage sets the amplitude of the voltage step that is applied to the probe. An analog switch then switches between this voltage and ground creating the frequency and duty cycle of the drive waveform, after which the voltage is fed

into a drive amplifier to drive the probe with a rectangular voltage waveform with up to 300 mA of current.

For the absolute mode of operation, the current through the drive coil, which is also the sense coil in this configuration, is the signal of interest. The current is sensed through a 1.0 ohm resistor in series with the coil. The voltage across this resistor is amplified through a software controlled programmable gain amplifier and then routed out a connector on the back of the board and connected through a cable to channel two of the analog-to-digital converter expansion board.

In the reflection mode of operation, the voltage across the sensing coil is the signal of interest. It is measured by a single-ended amplifier and then amplified by a software controlled programmable gain amplifier. The signal is then fed out the back of the card to channel one of the analog-to-digital converter.

The board is controlled by a microcontroller, which communicates with the PC across an 8-bit ISA bus and sets up the PEC card appropriately. The parameters on the card that are selectable are the drive waveform amplitude, frequency, and duty cycle and the gain of both programmable gain amplifiers. An 8-bit word is used to set the digital-to-analog converter. Another 8-bit word contains the gain settings for the programmable gain amplifiers.

The clock for the microcontroller is the 10 MHz clock from the ADC board. It was necessary to use the clock from the ADC board to synchronize the step voltage driving signal with the digitization of the ADC. If these were not synchronized, the sampling would take place at different locations on the waveform. When sampling occurred at one location for the null trace signal acquisition but was slightly shifted for subsequent traces, a significant error

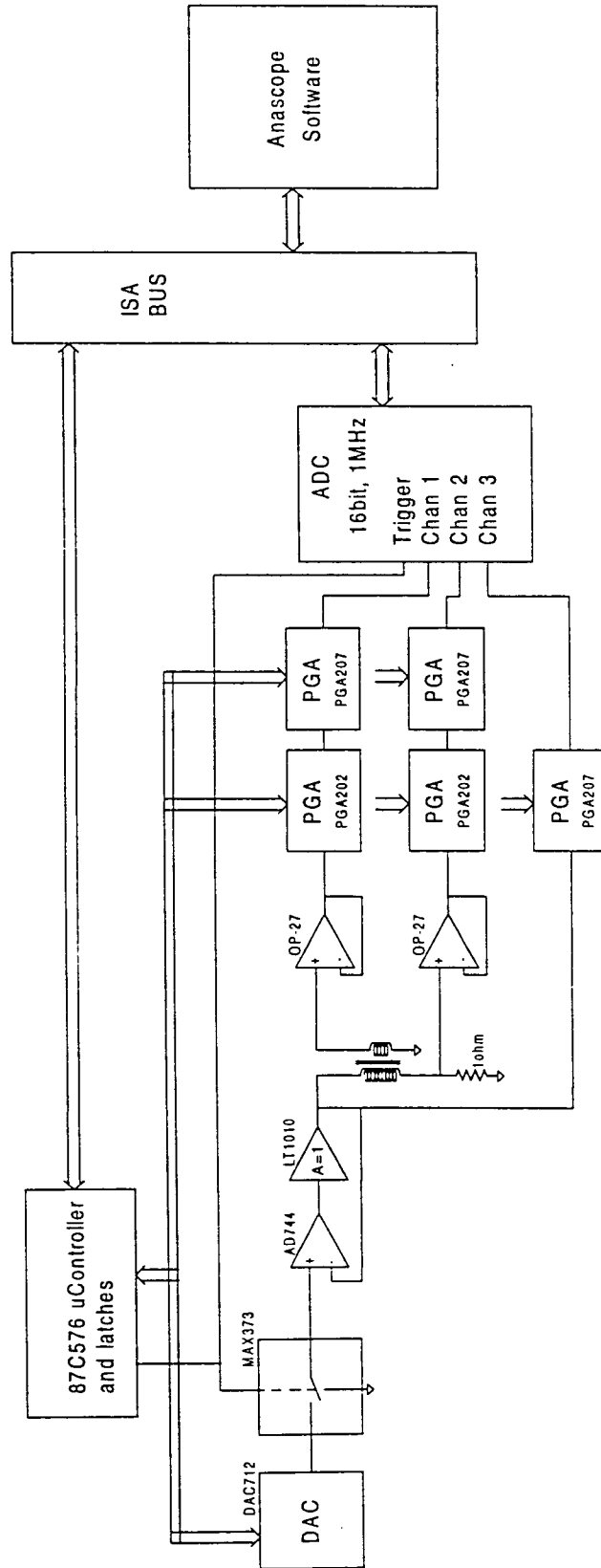


Figure 2.5. Block diagram of pulsed eddy current electronic hardware.

was observed. This was especially notable when the reflection mode was used because of the sharp rise time at the beginning of the waveform.

2.4. Analog-to-Digital Converter

The analog-to-digital converter is an off-the-shelf board from Analogic Corporation, model number 16-1-1. The heart of the board is a 16 bit converter with a 1 MHz sampling rate. This chip is mounted on a PC expansion board which mounts in a 16 bit ISA slot. Memory capable of storing 1 million samples is also present on the board to buffer data transfer across the bus.

2.5. Scanner, Stepper Motors, and Controller Board

The scanner, stepper motors, and controller board were adapted from a scanner originally developed for the Dripless Bubbler, an ultrasonic instrument. [7] The scanner is an indexing X-Y scanner capable of scanning a 34 cm by 12 cm area and was designed for lap joint scanning. The motor controller indexer is the Compumotor AT6400 model with the S series microstepping motors.

2.6. Personal Computer and Software

The personal computer, a PAC 486-66 from Dolch Computer Systems Inc., that was used to control the system is based on an Intel 486 processor operating at 66 MHz. It is housed in a lunchbox style case and allows for five 16-bit ISA expansion boards. Three of the expansion slots are used with this system: one each for the PEC board, ADC board, and the motor controller board.

The software is a Microsoft WindowsTM-based program written with Microsoft Visual C++ using the Microsoft Foundations Class. All of the control and display functions needed to scan a sample and acquire and display data are included.

The software has been an ongoing project and has been developed by several programmers. The data acquisition and signal display foundation was written by Mark Kubovich. The author then added the capability of the software to control the PEC board. After that, Sunil Shaligram added the scanning and imaging capabilities and Jerry Patterson refined the image display.

2.7. Constant Current Drive

After the constant voltage drive system had been built and tested, it was decided to test a constant current drive system. Some advantages of the constant current drive is that the constant current mode offers better time resolution, making discrimination of the location of flaws in the material easier. Using the constant voltage drive, the flaw signals are broadened by interaction with the time constant response of the coil. The variability from temperature fluctuations is reduced in some configurations because the eddy currents are induced by the current through the coil, not the voltage across the coil. In constant voltage mode, the current through the coil, and hence the induced eddy currents, vary with the impedance of the coil. Also, the theoretical modeling is easier because the impedance is measured directly, instead of measuring the admittance and then inverting it to get the impedance, as is done with the constant voltage drive.

Adding the constant current capability was accomplished by inserting an additional electronic circuit in-line between the PEC card and the probe to act as a transconductance

amplifier and convert the voltage drive level coming from the PEC card to a current drive. See Figure 2.6 for a schematic. The electronics to perform this function were designed and built by Technology Resource Group, L.C., in Des Moines, IA, and then modified by the author. Since the probes can have quite a large inductance (we have used some up to several millihenries), high voltage power supplies were needed to approximate a current step through the inductor. Positive and negative one hundred volt supplies were used.

Since the current through the coil is regulated in this constant current mode, a measurement of the voltage across the coil is required to sense the change in impedance of the coil. The circuitry provides for sensing this voltage and scaling it down to the required

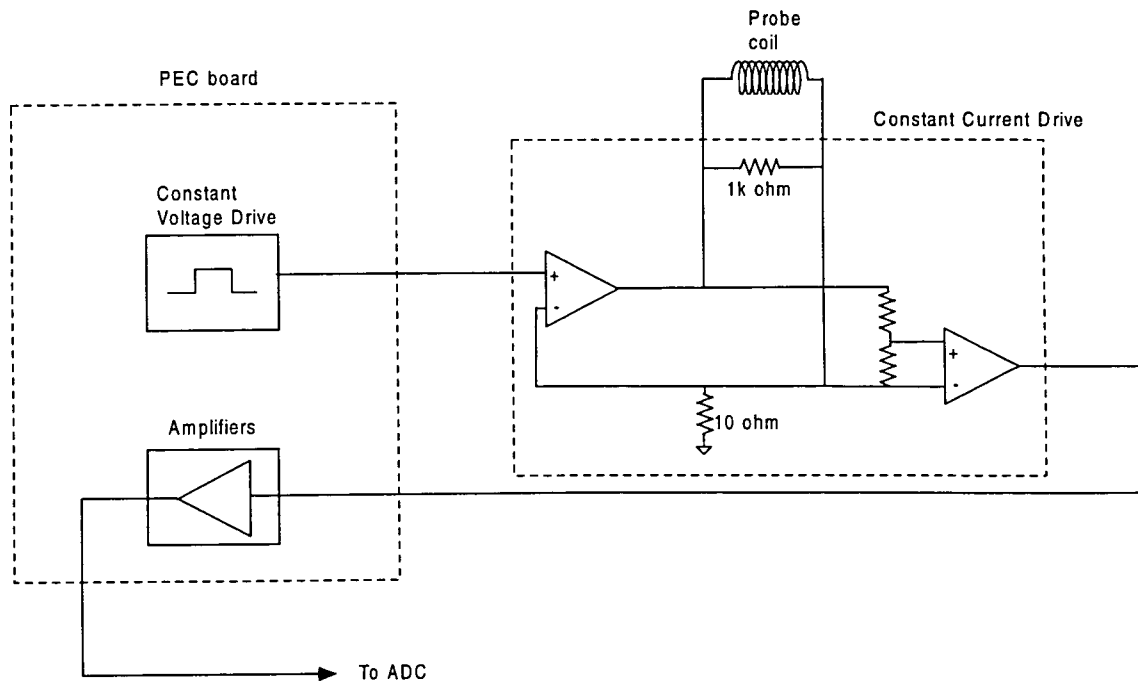


Figure 2.6. Schematic diagram of constant current drive.

voltage levels is also performed by this circuitry. The output signal is then fed into the PEC card where it is scaled under software control and fed into the ADC board.

2.8. Magnetic Sensor Circuitry

It was also determined that magnetic sensors could be beneficial for sensing deep corrosion, so another circuit was made that could be placed in line with the probe and used with the constant current drive or constant voltage drive. The magnetic sensor consists of a resistive bridge with two active giant magnetoresistive sensors in opposite legs of the bridge and two identical dummy sensors in opposite legs of the bridge that were shielded from the magnetic field. This sensor will be discussed in more detail in Chapter 4.

The electronics includes circuitry to bias the bridge sensor with a constant current and also to sense the differential output of the sensor. This output is then fed back to the PEC board where it can be scaled by software-controlled gain amplifiers and routed to the ADC board.

CHAPTER 3. COIL SENSOR: ABSOLUTE MODE

Operation of the PEC system with the constant voltage drive has been reported in several papers [2,4,5,6,8,9]. The focus of this study is on the use of the constant current drive.

3.1. Description

The constant current drive absolute mode coil is analogous to the constant voltage drive absolute mode. While the constant voltage mode drives the coil with a step voltage allowing the current through the coil to increase at rate determined by the inductance and series resistance time constant in the coil, the constant current mode drives the coil using a current step with a finite rise time. This current will induce eddy currents in the material. Any changes in these eddy currents due to a flaw in the material are sensed by the coil as a change in impedance, which is observed as a change in the voltage across the coil.

3.2. Theory

The theory for the response of a coil over a layered sample has been developed by Cheng, Dodd, and Deeds [10] for a single fixed frequency and applied to the pulsed eddy current problem by Rose, Uzal, and Moulder [11].

The impedance of the coil, Z_L , over layers of conducting material computed by the Cheng, Dodd, and Deeds theory is given by

$$Z_L(\omega) = K \int_0^{\infty} \frac{I(\alpha)^2}{\alpha^6} \left\{ 2\alpha h + (1 - e^{-\alpha h}) \left[\frac{U_{12}}{U_{22}} e^{-2\alpha h} (1 - e^{-\alpha h}) - 2 \right] \right\} d\alpha \quad (3.1)$$

where

$$K = -\frac{j\pi\omega N^2 \mu_0}{h^2(r_2 - r_1)^2}, \quad (3.2)$$

$$I(\alpha) = \int_{\alpha_1}^{\alpha_2} x J_1(x) dx. \quad (3.3)$$

U and H_n are 2 by 2 matrices determined by

$$U = H_{m-1} H_{m-2} \dots H_2 H_1, \quad (3.4)$$

$$(H_n)_{11} = \frac{1}{2}(1 + \beta_n) e^{(\alpha_{n+1} - \alpha_n) z_n}, \quad (3.5)$$

$$(H_n)_{12} = \frac{1}{2}(1 - \beta_n) e^{(\alpha_{n+1} + \alpha_n) z_n}, \quad (3.6)$$

$$(H_n)_{21} = \frac{1}{2}(1 - \beta_n) e^{-(\alpha_{n+1} + \alpha_n) z_n}, \quad (3.7)$$

$$(H_n)_{22} = \frac{1}{2}(1 + \beta_n) e^{-(\alpha_{n+1} - \alpha_n) z_n}, \quad (3.8)$$

and

$$\beta_n = \left(\frac{\mu_{n+1}}{\mu_n} \right) \left(\frac{\alpha_n}{\alpha_{n+1}} \right), \quad (3.9)$$

$$\alpha_n = \sqrt{\alpha^2 + j\omega\mu_n\sigma_n}. \quad (3.10)$$

The variables are defined as:

N = number of turns on coil,

h = height of coil,

r_2 = outer radius of coil,

r_1 = inner radius of coil,

z_n = interface depth between layers n and $n+1$,

n = layer number,

α = integration variable,

μ_n = permeability of layer n ,

σ_n = conductivity of layer n .

The theory of Cheng, Dodd, and Deeds was derived for an ideal coil and does not take into account the resistance of the coil windings or the parasitic capacitance of the coil. Also, to keep the coil from ringing when excited near its resonant frequency, a parallel resistor was added to the circuit, in parallel with the coil, to overdamp the response of the coil. All of these factors need to be added to the theoretical model. The equivalent circuit for the coil is modeled as shown in Figure 3.1.

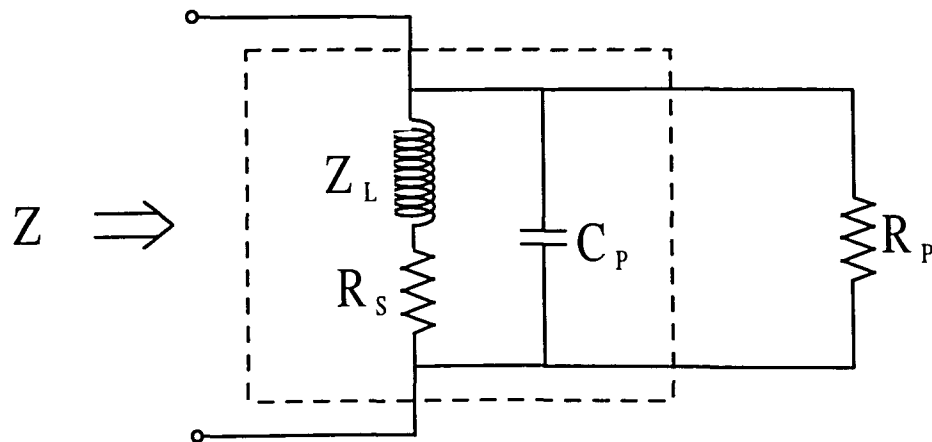


Figure 3.1. Schematic of the coil used for theoretical modeling. Z_L , R_S , and C_P are coil parameters and R_P is an external resistor. Z is the total impedance.

From this schematic, it can be seen that the impedance of the network can be described as

$$Z(\omega) = \left[\frac{1}{Z_C(\omega)} + \frac{1}{R_p} + \frac{1}{Z_L(\omega) + R_s} \right]^{-1}, \quad (3.11)$$

where

$$Z_C(\omega) = \frac{1}{j\omega C_p}, \quad (3.12)$$

$Z_L(\omega)$ is defined in equation (3.1), and $Z(\omega)$ is the impedance of the network.

This impedance, $Z(\omega)$, is then computed for a null (reference) area and a flaw area. The material for the null area is assumed to be an area without any flaws and is modeled as such. To find the impedance over a flaw location, the corrosion is simulated by inserting an air layer the same thickness as the corrosion. All layers are assumed to be infinite in extent laterally. The change in impedance is then computed as

$$\Delta Z(\omega) = Z_{flaw}(\omega) - Z_{null}(\omega), \quad (3.13)$$

where $Z_{flaw}(\omega)$ is the impedance of the coil network over the flawed portion of the material and $Z_{null}(\omega)$ is the impedance of the coil network over the non-flawed portion of the material where the null trace was acquired.

The change in impedance in the frequency domain is then transformed to the time domain using the Discrete Fourier Transform, computed using

$$\Delta Z[n] = \frac{1}{N} \sum_{k=0}^{N-1} \Delta Z(k) e^{j \frac{2\pi kn}{N}}. \quad (3.14)$$

Once the change in impedance is expressed in the time domain, it can be converted to a voltage waveform by multiplying it by the current through the coil network as in equation (3.14)..

$$\Delta V[n] = I * \Delta Z[n] \quad (3.15)$$

3.3. Experimental Setup

The setup was as described in Chapter 2, using the pulsed eddy current board with the external constant current drive discussed in Section 2.7.

The coil used was an absolute coil, where the coil that induces the eddy currents in the material is also the receive coil. It is an air core design with an inner diameter of 5.59 mm, an outer diameter of 10.67 mm, length of 2.54 mm, and 638 turns of 39 AWG wire.

For the simulated corrosion samples, two plates of 1 mm thick 2024 aluminum were used. This alloy was selected for the application of detecting corrosion in aircraft lap joints. To simulate corrosion, flat bottom holes were milled into one of the plates to various depths to simulate 50%, 30%, 20%, and 10% material loss in one of the plates. By placing the simulated corrosion in different positions, as shown in Figure 3.2, the signal could be analyzed for corrosion at three possible locations: the bottom of the top plate, the top of the bottom plate, and the bottom of the bottom plate.

3.4. Results

In this section, the results from theoretical predictions and experimental measurements are compared for the simulated corrosion sample shown in Figure 3.2.

A typical waveform for the signal starts at zero, rises to a positive peak, decreases, crossing zero to a negative peak, and then rises asymptotically back to zero. An example is

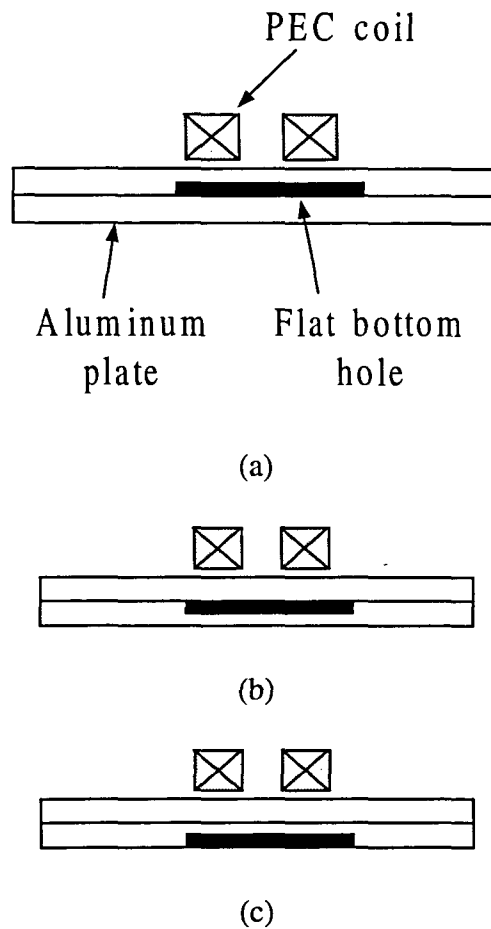


Figure 3.2. Samples using 2024 aluminum plates. Each sample uses two 1.0 mm thick plates stacked on top of each other. The flat bottom hole which simulates corrosion is shown in the bottom of the top plate (a), the top of the bottom plate (b), and the bottom of the bottom plate (c).

shown in Figure 3.3. It has been shown that for the constant voltage case the signals can be scaled by normalizing to the peak height and zero crossing so that they all fall on top of each other. This implies that the two parameters of most interest are the zero crossing and the peak height and this has been demonstrated by Moulder et al. [8].

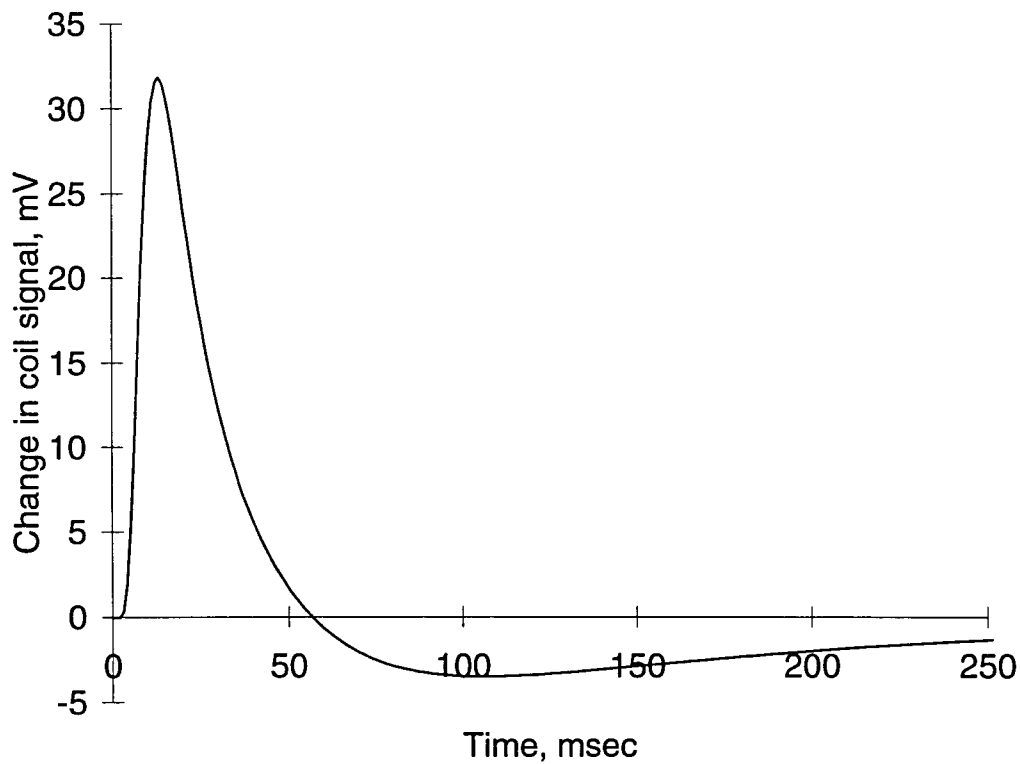


Figure 3.3. Characteristic pulsed eddy current signal.

In Figure 3.4, experimental and theoretical results for corrosion on the bottom of the top layer are plotted. Agreement between experiment and theory is very good, with less than 6% disagreement in peak height. Note that at the beginning of the signals there is a flat line at zero for approximately 9 μ s at the beginning of the trace due to the rise time of the coil. This is a result of the configuration of the sensing electronics. Since the coil is excited with a current step a high voltage spike occurs across the coil during the first few microseconds during which the current in the coil is rising. Once the current has reached its constant level, the voltage drops to the dc level determined by the series and parallel resistance in the coil. When this high spike occurs, the signal is clipped before it is amplified and sent to the ADC.

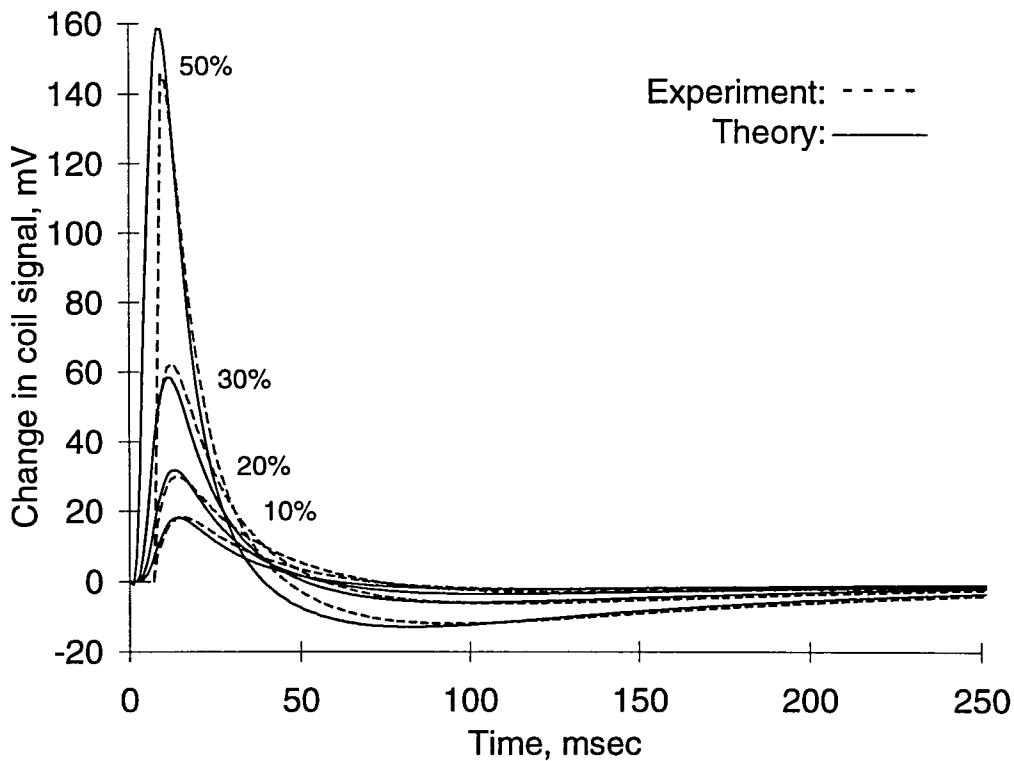


Figure 3.4. Comparison of theory and experiment for increasing amounts of corrosion located on the bottom of the top plate.

This allows the signal to be amplified more to maximize the usable resolution of the ADC. Because the noise floor is largely affected by the noise floor of the ADC card, the signal to noise ratio of the signal is also increased by this strategy. Thus, when the trace is subtracted from the null trace to get the flaw signal, the difference is zero. This is most pronounced for the 50% corrosion sample. For the rest of the samples, the peak of the signal is not affected. The signals look very similar in shape to the constant voltage response referred to in reference 5, although the pulses are narrower and occur earlier in the time than is the case for constant voltage drive.

Calculations and experiments were also performed for the case of corrosion on the top of the bottom layer, shown in Figure 3.5, and on the bottom of the bottom layer, shown in Figure 3.6, with similar results. For both locations, theory is in good agreement with experiment, generally agreeing within 15%.

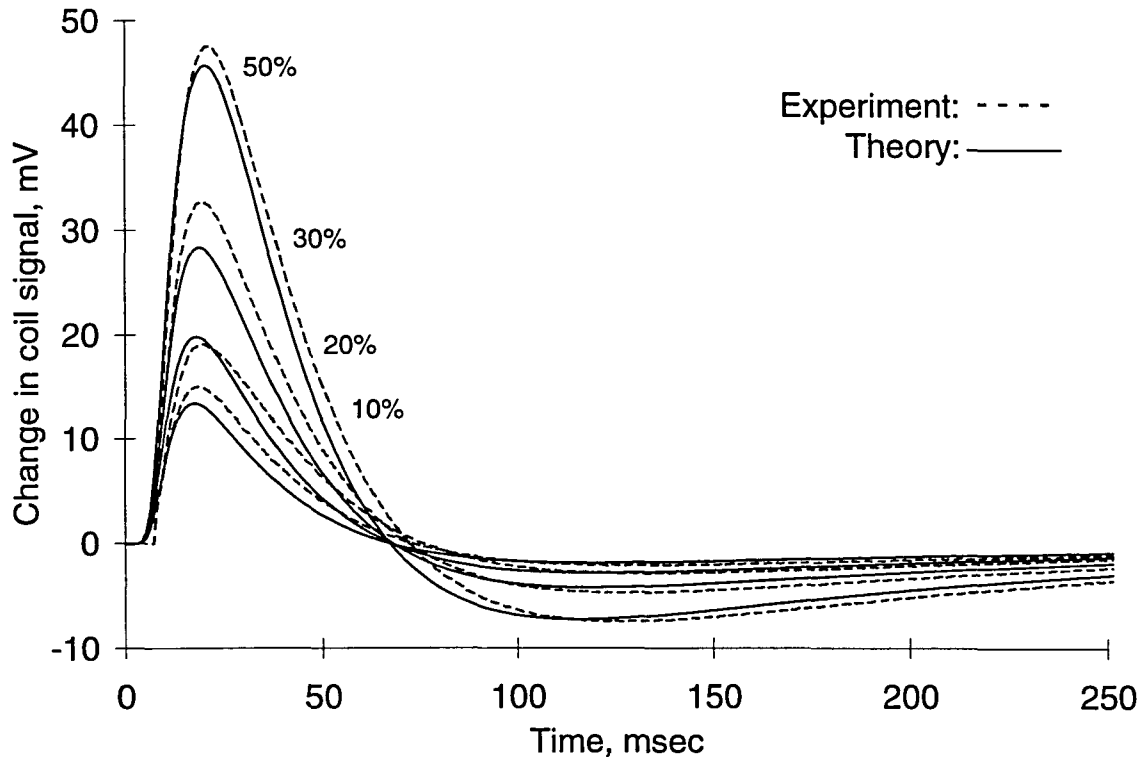


Figure 3.5. Comparison of theory and experiment for increasing amounts of corrosion located on the top of the bottom plate.

Comparing the signals from the three corrosion locations the following observations can be made. First, the deeper the corrosion is in the material, the further out in time the zero crossing occurs. The corrosion on the bottom of the top layer has the zero crossing occurring earliest in time and the corrosion on the bottom of the bottom layer has the zero crossing occurring the latest in time. Second, for a specific corrosion location, the peak height

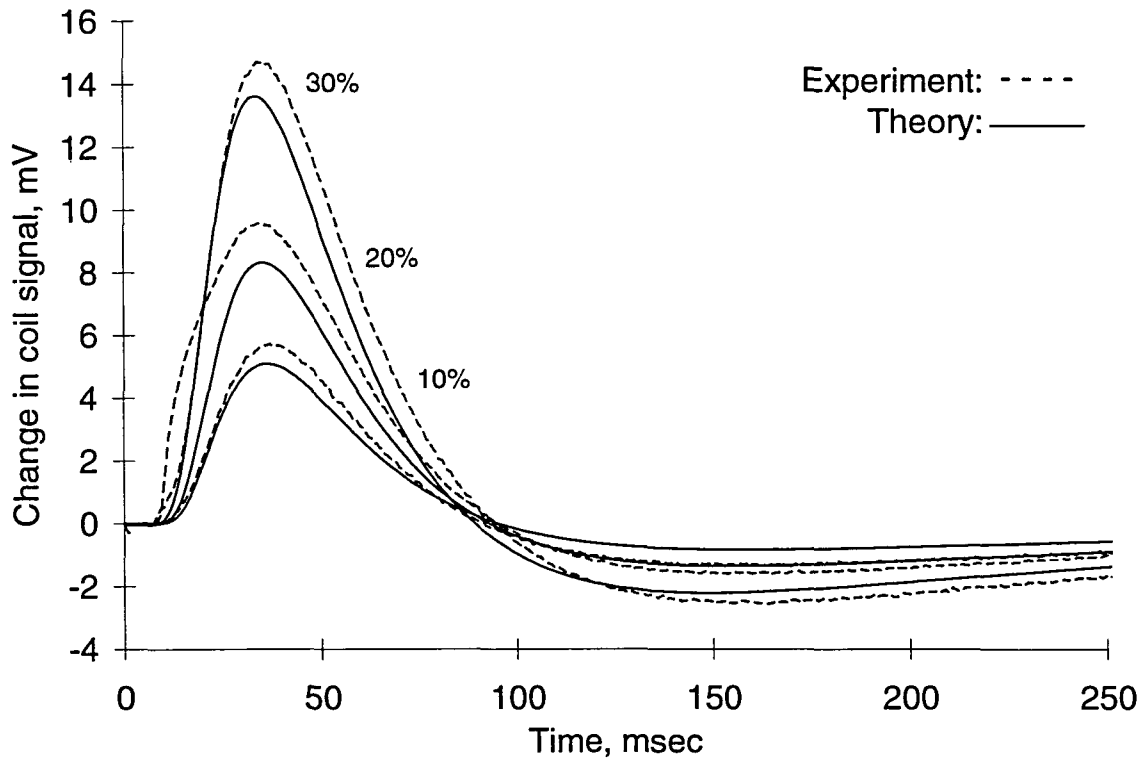


Figure 3.6. Comparison of theory and experiment for increasing amounts of corrosion located on the bottom of the bottom plate.

increases with the amount of corrosion. That is, the signal always increase in amplitude from 10% corrosion on up to 50% corrosion. Third, the signal amplitude decreases as the corrosion is located deeper in the sample. For example, for any amount of corrosion, the amplitude is largest on the bottom of the top layer, decreases on the top of the bottom layer, and is the smallest on the bottom of the bottom layer.

3.5. Conclusions

The pulsed eddy current system which was set up for constant voltage drive was modified to allow for a constant current drive to operate the probe in the absolute mode.

Using the Cheng, Dodd, and Deeds theory as a basis, a theoretical model was created and coded to simulate the response. Experiment and simulation were compared for two plates of 1 mm thick 2024 Aluminum with flat bottom holes in various location to simulate corrosion. This configuration is representative of an aircraft lap joint. The theory was in good agreement, generally within 15%, with the experimental results for corrosion located in all three of the possible locations.

CHAPTER 4. MAGNETIC SENSORS FOR DEEP PENETRATION

4.1. Description

Previous configurations described in this study have used a coil sensor for the probes and have been driven with a constant voltage or a constant current drive. A variation on this setup is to use a magnetic sensor in place of the coil sensor. Unlike the coil sensors, a magnetic sensor senses the magnetic field in the center of the coil. Also, these sensors are primarily sensitive along one axis and have minimal sensitivity to fields orthogonal to this axis, whereas the coil is sensitive to all the flux threading the coil.

The purpose of the work described in this chapter is to compare the ability of a giant magnetoresistive (GMR) sensor equipped probe with an absolute mode probe, which uses a coil sensor, to detect corrosion that is buried deeply in 6.3 to 12.7 mm thick 2024 aluminum plates.

4.2. Motivation

Using eddy currents to detect flaws buried deeply in a conducting material has always been a difficult problem. This is due, in part, to the fact that deep penetration requires low frequencies so that the skin depth is large enough for the eddy currents to penetrate into the material to the depth of the flaw. Using an approximation of skin depth, δ , given by

$$\delta = \frac{1}{\sqrt{f\pi\mu\sigma}} \quad (4.1)$$

where f is the frequency of excitation, μ is the permeability, and σ is the conductivity of the material, it can be seen that the depth of penetration of the eddy currents into the material is inversely proportional to the square root of the frequency of excitation. The depth of

penetration is also limited by the permeability and conductivity of the material. Since skin depth is defined for a plane wave incident on the surface of the material, this is only an approximation. The actual depth of eddy current penetration is also affected by the probe size and is limited to approximately the radius of the coil.

Aluminum is a common material used in the aircraft industry and was used for the experiments in this section. For 2024 Al which has a permeability of $4\pi \times 10^{-7}$ H/m and a conductivity of 18.53 MS/m, a continuous wave frequency of 83 Hz is required to achieve a skin depth of 12.7 mm.

A significant advantage of the pulsed eddy-current system for deep penetration when compared to the traditional fixed-frequency instrument is that the probes are easier to build and design. For a continuous wave system operating at 100 Hz (which would be required to reach depths of 6.3 mm to 12.7 mm) an impedance of approximately 50 ohms would be required to operate with traditional eddy-current instruments, because a matched bridge of approximately 50 ohms is required. This would translate to an inductance of 80 mH if the inductor were perfect. However, in a practical design, the resistance of the wire would dominate the impedance of the coil. For a coil of similar dimensions to the one used with the pulsed eddy-current system with a total impedance of 50 ohms, 1750 turns would be required. The inductance would be 30 mH and the DC resistance of the wire would be 34 ohms out of the total of 50 ohms. This makes it difficult to fabricate a coil to operate at these depths with traditional eddy-current instruments. Pulsed eddy-current systems do not have this impedance limitation, since they can easily operate with lower inductance coils.

The eddy current response can be detected by a coil sensor, as demonstrated previously in Chapter 3, or by a magnetic sensor. According to Faraday's law of electromagnetic induction,

$$V = -N \frac{d\Phi}{dt}, \quad (4.2)$$

where N is the number of turns and Φ is the flux coupling the coil; thus the voltage induced in a coil is proportional to the rate of change of flux linking the circuit.

A magnetic sensor, however, senses the magnetic field directly and not its derivative. Thus, the signal will not fall off with depth as quickly as the coil sensor. Hence, when sensing flaws at these greater depths, the magnetic sensors have a distinct advantage over the coil sensors because the signal is larger and it does not drop off as quickly with depth.

4.3. Theoretical Results

When comparing the fall off of the signal with depth for a pulsed eddy-current system, it is not obvious how the signal should fall off. Because of this, simulations were performed for the magnetic sensor and the coil sensor configurations to determine the fall off of the two sensors. The simulation for the coil sensor is based on the Cheng, Dodd, and Deeds formulation [4] applied to the transient pulsed eddy-current system by Rose, Uzal, and Moulder [5]. The modeling software used was MPEC version 5.0 created by Cheng-Chi Tai. The magnetic sensor simulation is based on the formulation by Bowler and Harrison [6] and Johnson [7]. The software for the magnetic sensor simulation was written by Bowler.

The simulation results described here are for a panel of 2024 Al with 10% metal loss. To allow for comparison between the magnetic signals and the current signal from the coil sensor, the signals are normalized to $\Delta H/H$ and $\Delta I/I$.

The normalized peaks of these signals versus thickness of the sample, hence depth of penetration, are plotted in Figure 4.1. Looking at Figure 4.1 (B), it can be seen that the signal from the magnetic sensor is three times as strong as the coil sensor for 4 mm thickness of the sample and increases to ten times the strength for a 15 mm thickness.

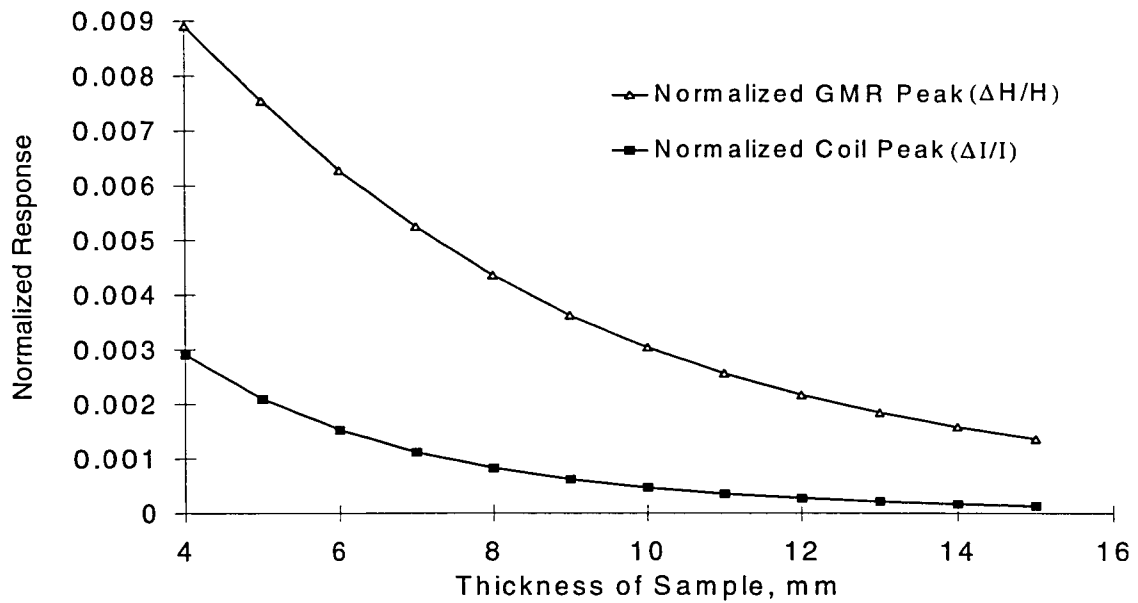
4.4. Giant Magnetoresistive Sensors

4.4.1. Description

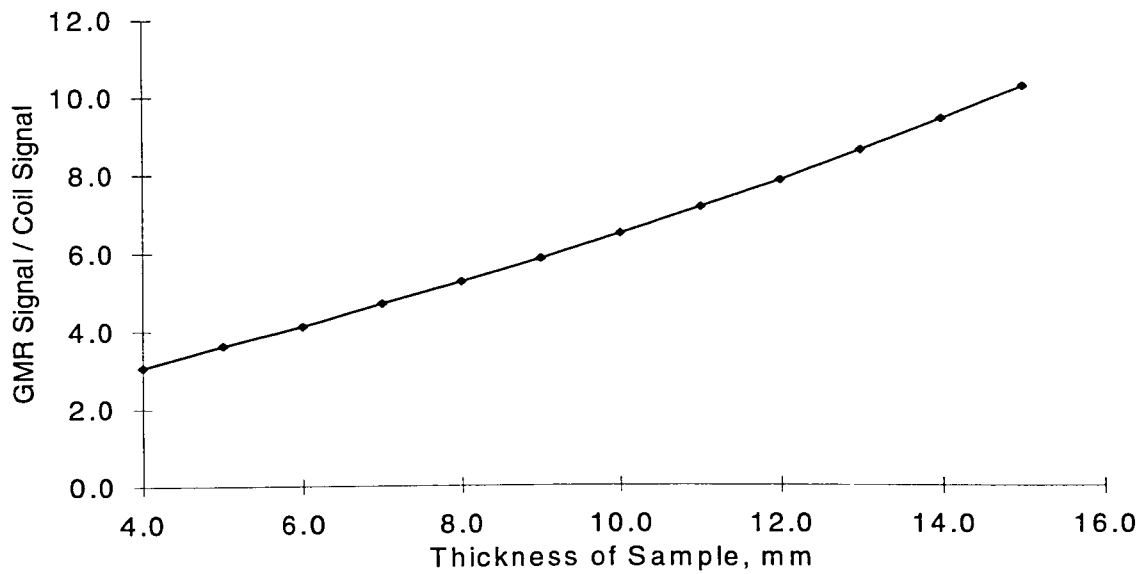
The magnetic sensor used in this study is based on the giant magnetoresistive effect and is shown schematically in Figure 4.2. The sensor is made up of four GMR elements arranged in a resistive bridge configuration. Two of the elements are located between a pair of flux concentrators and change in accordance with the applied magnetic field. These two elements are located on the opposing sides of the bridge. The other two elements are shielded from the magnetic field and are used to balance the bridge. This sensor has a directional sensitivity along the longitudinal axis of the 8 pin SOIC package and very little sensitivity to orthogonal fields.

Giant magnetoresistive (GMR) sensors produce a change in resistance of the sensor when a magnetic field is applied. A GMR sensor is constructed of alternating layers of soft magnetic and nonmagnetic materials which are a few nanometers thick.

The resistivity of the magnetic conductor layers is dependent on the mean free path of the electrons. The shorter the mean free path, the higher the resistivity. The mean free path is affected by spin-dependent scattering. Since the scattering of electrons is affected by the relative alignment of the conduction electron spins and the magnetic moments in the material,



(A)



(B)

Figure 4.1. Theoretical predictions of the coil sensor and GMR sensor for detecting 10% corrosion on the bottom of a 2024 Al panel. (A) The peak of the normalized signal vs. thickness of sample. (B) Comparison of the signal strength between the two sensors.

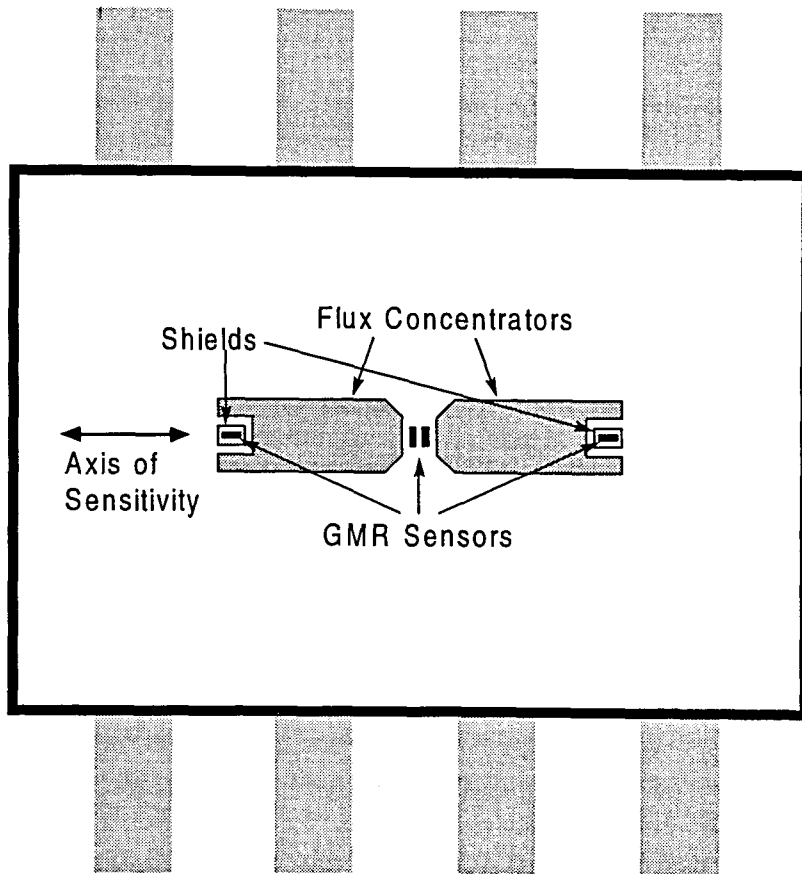


Figure 4.2. Schematic of the GMR sensor.

the greater the misalignment between the spins and the magnetic moment, the shorter the mean free path will be.

As an electron enters the first magnetic layer, its spin is brought into alignment with the magnetic moments of that layer. The electron passes through the conduction layer to the next magnetic layer. If the spin of the electron is aligned antiparallel to the magnetic moment, much scattering results. These interactions continue through several layers. If the magnetic moments of the magnetic layers are in parallel alignment, the scattering effect is not as large, and thus the resistance is lower.

The antiparallel alignment of alternating layers is accomplished by passing a bias current through the sensor which causes the magnetic moments of the layers above and below the conducting layer to be in antiparallel alignment. When the sensor is acted on by an external magnetic field, this external field will overcome the effects of the bias current and align the magnetic layers in parallel [12, 13].

This sensor is operated as a standard resistive bridge. The bridge sensor is biased with a current source and the amplified differential output of the bridge is the signal of interest.

4.4.2. Comparison to other sensors

There are other sensors which could have been chosen and have been used to detect the magnetic field in eddy current probes. Two of the most common are Hall probes and superconducting quantum interference devices (SQUIDs). Use of Hall probes for the pulsed eddy current application has been investigated by Bowler and Harrison [14], Johnson [15], and Waidelich [16], as well as others. Work has recently been reported on SQUIDs by Podney and Moulder [17]. A magnetoresistive sensor configuration has also been used in a fixed frequency eddy current measurement [18] to detect cracks.

Although SQUIDs are the most sensitive of the listed magnetic sensors, their major drawback is that they must be cryogenically cooled and cannot operate near room temperature. This limits its use in the field inspection setting.

Hall probes are also small, sensitive devices which are easily implemented and operate well at room temperature. These sensors have been used quite extensively in pulsed eddy current applications. GMR sensors are a newer technology and have not been

thoroughly investigated for pulsed eddy current use. Since they are more sensitive than Hall devices, it is desirable to investigate further how they would perform in a pulsed eddy current system.

4.5. Experimental Results

4.5.1. Experimental Setup

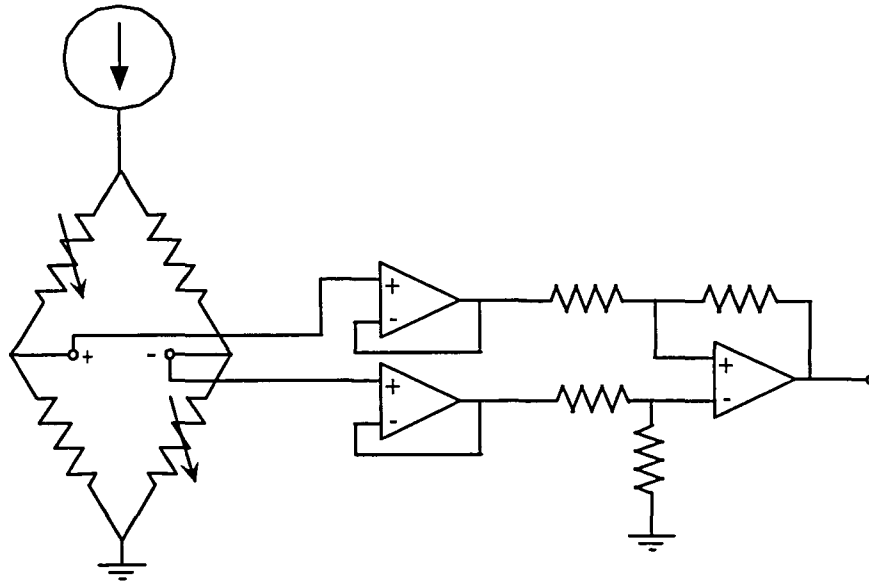
4.5.1.1 Electronics

The pulsed eddy current system described in Chapter 2 was used for these experiments with modifications to the hardware to accommodate the GMR sensor. This consisted of electronics to create a bias current through the sensor bridge and a differential amplifier configuration to extract the differential output of the bridge. The GMR and associated electronics are shown schematically in Figure 4.3 (A).

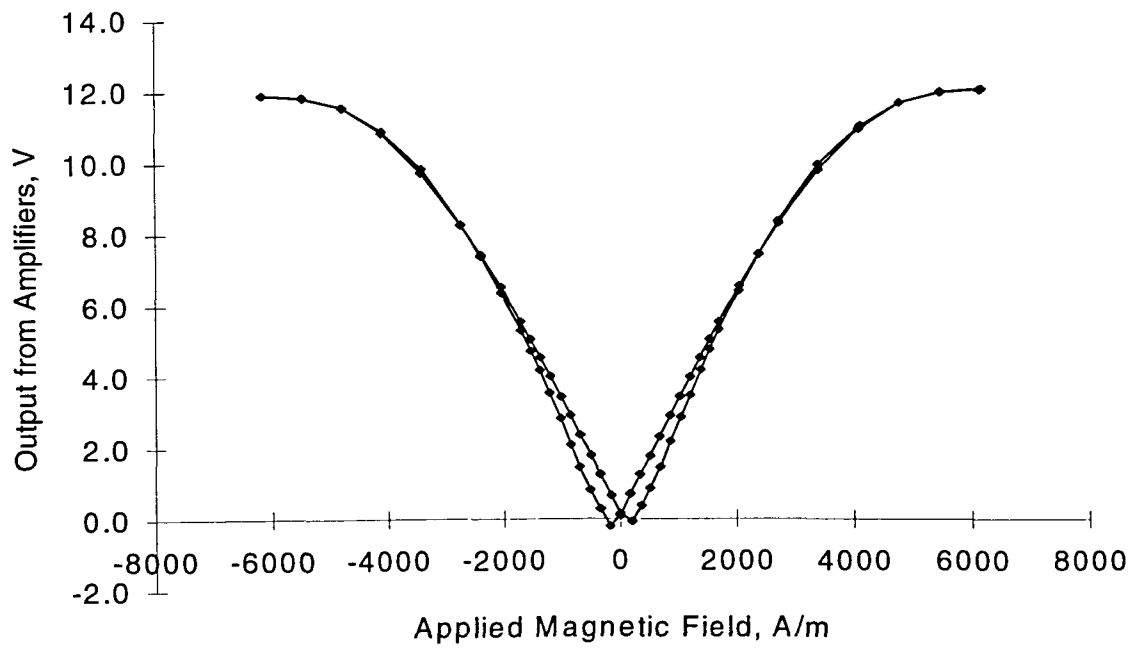
Due to the nature of the GMR effect, the sensor is not sensitive to the sign of the magnetic field. Thus, the output from the sensor and associated electronics is a unipolar response sensitive only to the magnitude of the component of the magnetic field parallel to the axis of sensitivity of the sensor. The response of the sensor has been experimentally determined, as shown in Figure 4.3 (B).

4.5.1.2 Probe Design

As discussed above, the impedance of the probe is not as critical as for the traditional fixed frequency eddy current case, where the impedance of the probe needs to be approximately 50 ohms at its operating frequency. This allows for a probe which is easier to design and build. The probe used for the pulsed eddy-current system is shown in Figure 4.4.



(A)



(B)

Figure 4.3. Design of GMR sensor electronics. (A) The circuitry used to drive the bridge sensor and sense the output signal. (B) The output response of the sensor due to magnetic stimulus.

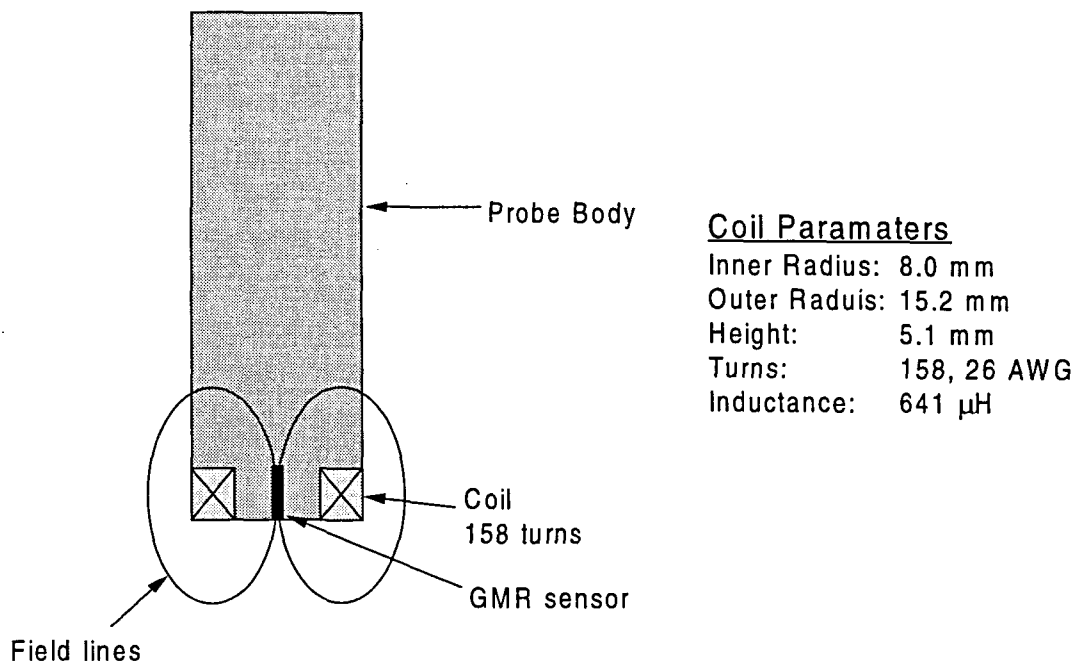


Figure 4.4. GMR probe design for the pulsed eddy current system.

4.5.1.3 Test Sample

Two test sample sets were used. The first set consists of two plates of 2024 Al, 6.35 mm thick. Each plate had flat bottom holes machined in the bottom side of the plate with depths ranging from 50% to 5% of the total plate thickness (refer to Figure 4.5). The reference trace is taken at the location labeled “null” in the figure.

The second sample used the same two plates, except with a second plate on top which did not have any machined defects in it. This resulted in a sample with a total thickness of 12.7 mm. The flat bottom holes on the bottom the sample then represented 25% to 2.5% of the total plate thickness (refer to Figure 4.6).

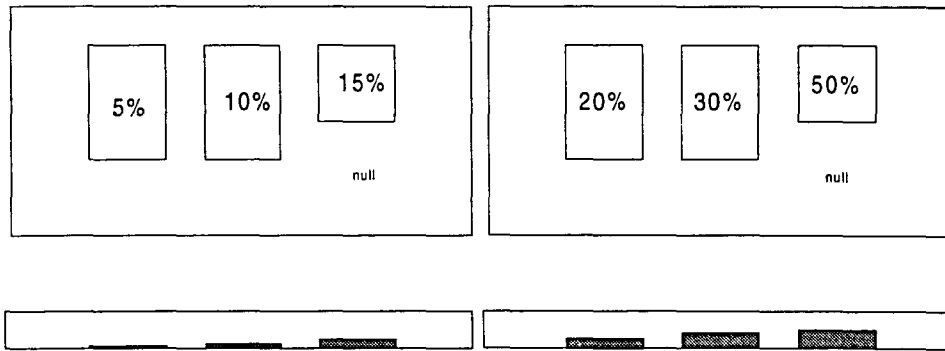


Figure 4.5. The 6.35 mm thick sample with flat bottom holes on the bottom of the plate to simulate corrosion.

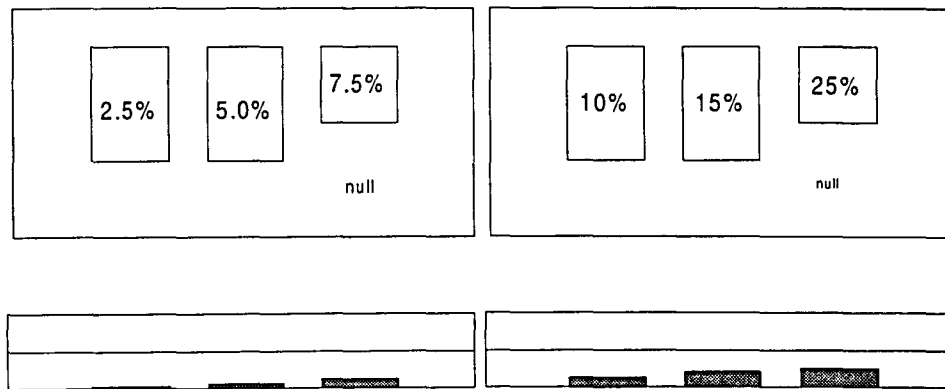


Figure 4.6. The 12.7 mm thick sample is made up of two 6.35 mm plates with flat bottom holes on the bottom of the sample to simulate corrosion.

4.5.2. Experimental Results

The probe was tested in both the absolute coil sensor mode, where the same coil is used as both drive and receive coil, and also in the magnetic sensor mode, where the eddy-currents are induced by the coil and the change in the magnetic field incident on the GMR sensor is the received signal. These two configurations were used to detect simulated corrosion (flat bottom holes) on the bottom of 6.35 mm thick and 12.7 mm thick 2024 Al panels. The procedure was to take a reference, or null, trace on the “null” location where there is no metal loss. The probe was then moved to the middle of an area of simulated

corrosion where a second trace was acquired, which is automatically subtracted from the null trace by the software.

For the 6.35 mm thick panel, both probes could detect the entire range of simulated corrosion present in the sample, ranging from 5% to 50% of the total thickness. The signals are shown in Figure 4.7.

The normalized signal from the magnetic probe for 10% corrosion is 3.55×10^{-3} for the magnetic sensor and 1.23×10^{-3} for the coil sensor. Thus, the signal strength for the magnetic sensor is 2.9 times the strength of the coil sensor. This is in reasonable agreement with the predicted ratio of 4.1 in Figure 4.1 (B).

Using the GMR sensor mode, the probe was fixed in the scanning fixture and the sample was scanned. The result is shown in Figure 4.8, illustrating the ability of the magnetic sensor-based system to image areas of corrosion using the same software developed for the coil-based system.

Measurements were also taken on a sample of 2024 Al, 12.7 mm thick, with simulated corrosion ranging from 2.5% to 25% on the bottom of the panel. As shown in Figure 4.9, both sensors were able to detect the 25%, 15%, and 10% corrosion. However, the GMR sensor was more sensitive and was able to detect levels of corrosion down to 2.5% as well.

As expected, the signal from the GMR sensor was stronger than the coil sensor. For 10% corrosion, the normalized peak signal level from the GMR sensor was 1.9×10^{-3}

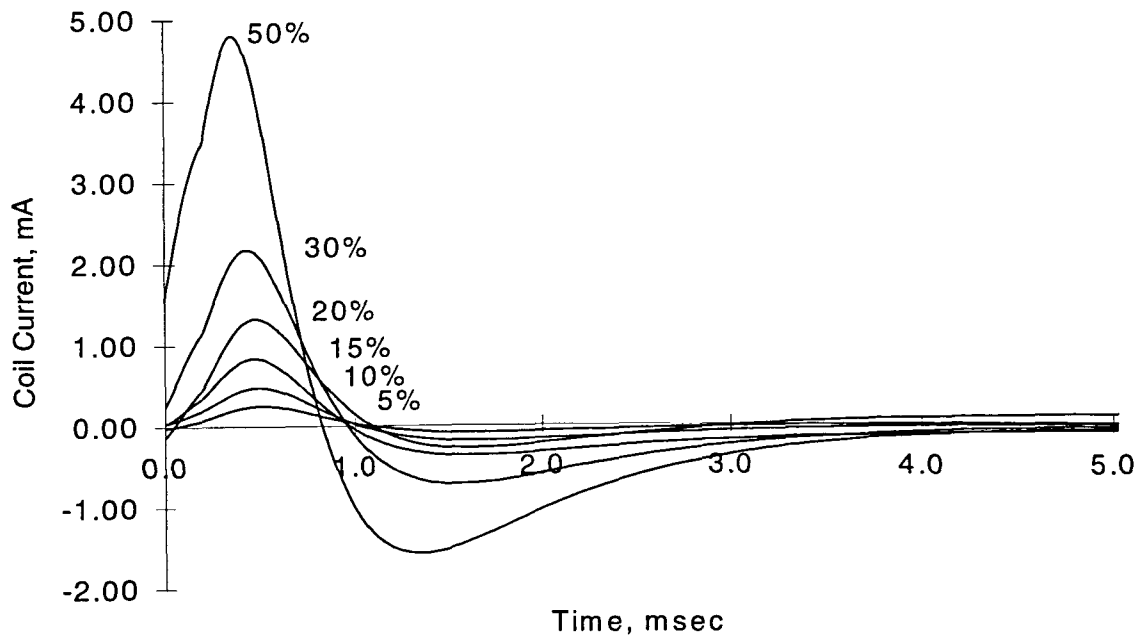
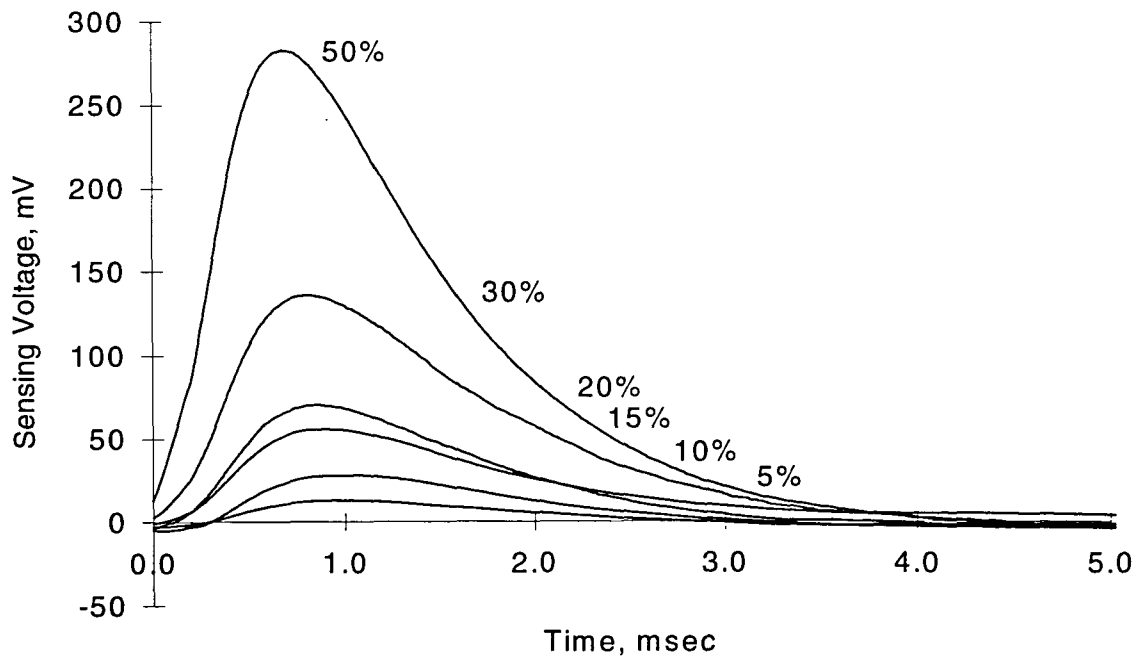


Figure 4.7. Signals for simulated corrosion on the bottom of a 0.250" panel of 2024 Al for the GMR sensor (A) and the coil sensor (B).

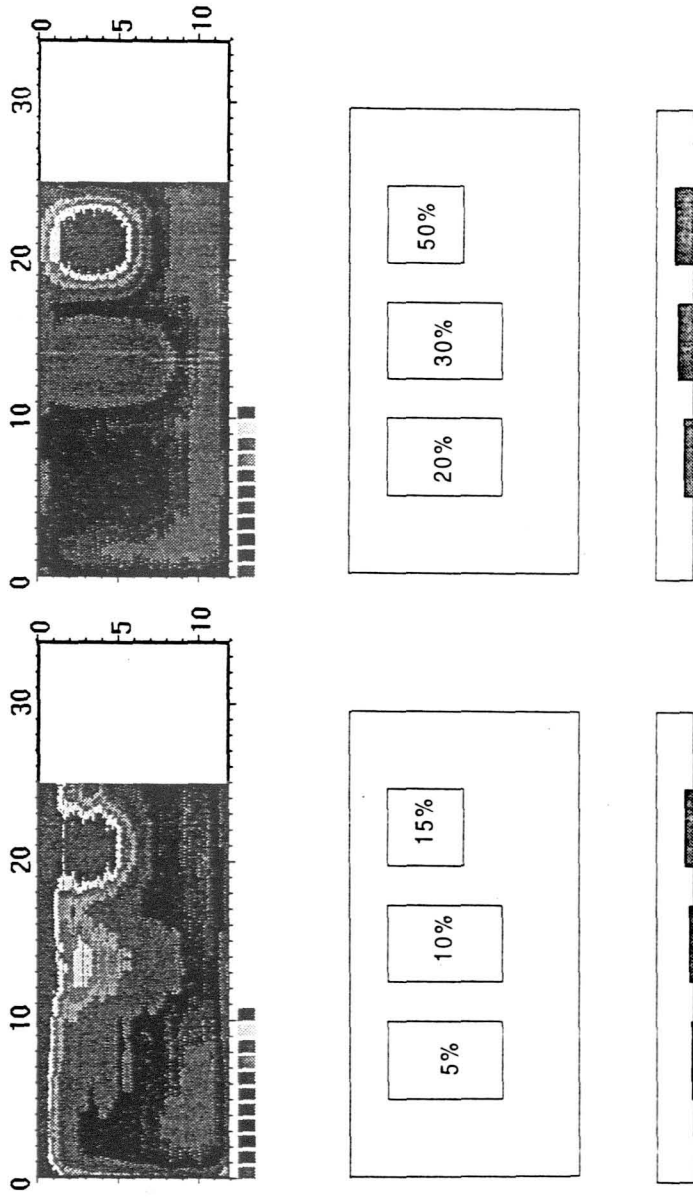
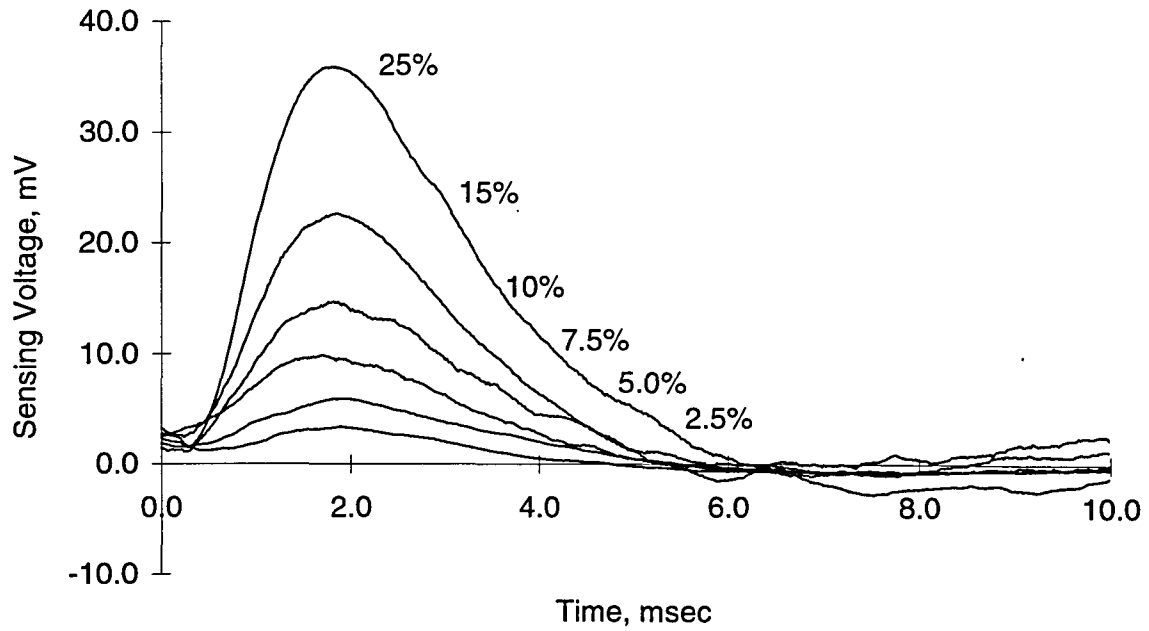
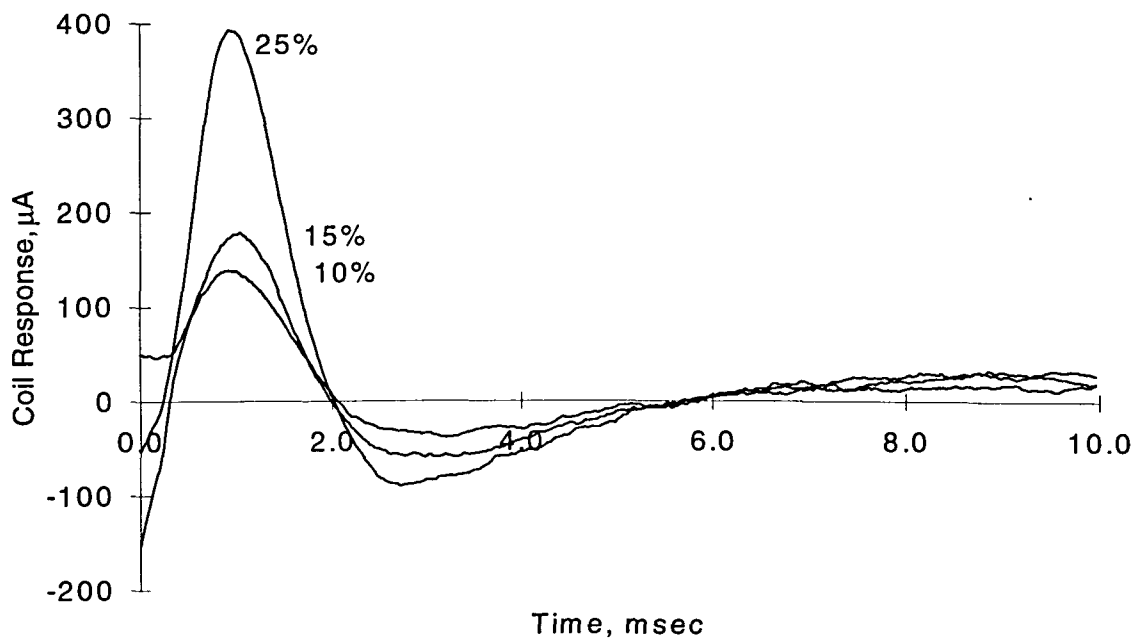


Figure 4.8. Scanned images using the GMR probe to detect simulated corrosion on the bottom a 0.250" thick panel of 2024 Al.



(A)



(B)

Figure 4.9. Signals for simulated corrosion on the bottom of a 0.500" panel of 2024 Al for the GMR sensor (A) and the coil sensor (B).

while the normalized peak signal level from the coil sensor was 0.257×10^{-3} . Thus the signal from the GMR sensor is 7.4 times the strength of the coil sensor. This is in good agreement with the predicted ratio of 8.4 in Figure 4.1 (B).

4.6. Conclusions

The ability of a giant magnetoresistive sensor to detect corrosion through thick plates of aluminum was investigated. First, it was determined by theoretical calculations that the signal from the GMR sensor is stronger than the coil sensor at deep penetration levels. Since this is true in the continuous wave approach and pulsed eddy-currents are a measurement containing a range of frequencies, this general trend was expected when the sensor was used in a pulsed eddy current instrument.

Given the stronger signal, it was expected that the GMR sensor would be significantly better at detecting deeply buried corrosion. This was verified experimentally by looking at corrosion on the bottom of 6.35 mm thick and 12.7 mm thick 2024 Al plates. For the case of corrosion on the bottom of the 12.7 mm thick plates, the GMR sensor performed markedly better. Its signal level was approximately 8 times the strength of the coil sensor and it was able to detect corrosion down to 2.5%. The coil sensor was only able to detect greater than 10% metal loss.

These results demonstrate that for deep penetration using pulsed eddy currents, the magnetic sensor is preferred over a coil sensor. It is clear that the giant magnetoresistive sensor performed well as a magnetic sensor for pulsed eddy current detection of corrosion, owing to its sensitivity, ease of use, and compactness.

CHAPTER 5. CONCLUSION

5.1. Summary

A system to measure flaws in conducting materials was designed and built using the pulsed eddy current method of nondestructive evaluation. The custom pulsed eddy current electronics in the system were originally designed and built by the author as an expansion board to a portable computer to operate in the constant voltage mode with either an absolute mode or reflection mode coil sensor. It worked well and was the basis of several experiments as described in Chapter Two.

To further extend the capabilities of the instrument to operate in a constant current drive mode, which excites the coil with a step current instead of a step voltage, an external box was added to the system which allowed the instrument to operate in a constant current mode with either an absolute mode or reflection mode coil sensor.

The operation of this instrument using the absolute mode was described in Chapter 3. Computer code to perform theoretical predictions for the case of corrosion in layers of conducting material was written. Experiments were then performed with the instrument to detect corrosion in the simulated lap joints of aircraft skin at three locations in the joint: on the bottom of the top layer, on the top of the bottom layer, and on the bottom of the top layer. The measurements were in good agreement with theory and the peak amplitudes agreed within 15%. This demonstrated the ability to detect and locate corrosion in lap joints.

Another area that we wished to investigate was deep penetration of metal. It is difficult to sense flaws buried deeply in metals because the signal peak for the same size flaw falls off exponentially with depth into the material in which the flaw is located. It was shown

that a magnetic sensor would yield a stronger signal than the coil sensor for these depths, due to the fact that the coil responds to the time derivative of flux and the magnetic sensor responds to the magnetic field directly. The instrument was modified to incorporate a magnetic sensor based on the giant magnetoresistive effect in addition to a coil sensor. The GMR sensor worked well and was able to detect corrosion as small as 2.5% of the total thickness on the bottom of a 12.7 mm thick sample, whereas the coil sensor could only detect 10% corrosion at the same depth. The normalized signal strength for the GMR sensor was almost 8 times the strength of the coil sensor signal.

5.2. Future Work

Following the successful conclusion of these experiments, it is appropriate to consider what may be done in the future to further enhance the performance of the instrument and extend its capabilities. First, it has become apparent that redesigning for the next generation of electronic hardware would be beneficial. The new version should include several improvements.

As is desirable with almost all instruments that deal with limits of detectability, benefit can be gained by increasing the signal-to-noise ratio, which will make the instrument able to detect even smaller amounts of corrosion and smaller cracks more accurately. One change which would lower the noise floor is to use programmable gain amplifiers with a lower input noise figure. Those used in this instrument are known to be a cause of excessive noise and have occasionally been bypassed with a fixed gain amplifier to lower the noise floor. If the card were moved external to the portable computer, noise from the computer

could be reduced but the trade-off is that the instrument would become more bulky and require an extra box.

The card should also be able to drive a wider range of probe configurations. Constant current and constant voltage drive should both be available on the card. The ability to use coil sensors in absolute mode, reflection mode, and with an external sensor should all be accommodated without having to add an external box, as is now the case.

It is also planned to replace the analog-to-digital converter expansion board, which costs about \$4000 at the present time, with an ADC integrated on the pulsed eddy current card itself. A digital signal processor could be added which would read directly from the ADC and process the signals. Currently there is a bottleneck with the current ADC card transferring all the data it acquires across the ISA bus. If the DSP could process the data and only send the final results to the WindowsTM environment, this bottleneck could be eliminated and the computer would not be required to perform signal processing operations.

More future work that should be pursued is to explore the detection of cracks under thick layers of metal. The ability to detect corrosion in thick materials was demonstrated in this study but the instrument's performance on cracks was not tested. There are several applications in the aircraft industry that would benefit by being able to detect deep cracks this way.

APPENDIX A. CODE FOR ABSOLUTE COIL SENSOR THEORY

```

C      Constant curent simulation for PEC.
C      William Ward
C      April 24, 1997
      INTEGER N
      DOUBLE PRECISION h1, h2, rin, rout, h, rb
      INTEGER NumL, p, pStop, CorLayer, count
      DOUBLE PRECISION z(0:10), Pi, wStop, wStart, wStep, mur(0:10)
      DOUBLE PRECISION muo, sigma(0:10), aStart, aStop, aStep
      REAL xIntegration
      DOUBLE PRECISION w, freq, a, xStep, xStart, xStop, f(0:500)
      DOUBLE COMPLEX K1, K, C1, C2, C3, C(0:5000), Sum1, Sum2
      DOUBLE COMPLEX C2a, C2b
      DOUBLE COMPLEX an(0:10), Bn(0:10), I(0:5000)
      DOUBLE COMPLEX H11(0:10), H12(0:10), H21(0:10), H22(0:10)
      DOUBLE COMPLEX T11(0:10), T12(0:10)
      DOUBLE COMPLEX T21(0:10), T22(0:10)
      DOUBLE COMPLEX U11, U12, U21, U22, Z1(1:3,0:500)
      DOUBLE PRECISION Current
      INTEGER m, kloop, nloop, NumPoints
      DOUBLE PRECISION temp, Sum, Vn(0:500)
      REAL tStart, tStep, tStop, Volt, V(0:500), amp, Icoil
      INTEGER tCount, tCountStop
      DOUBLE PRECISION Cpar, Rp, Rs
      DOUBLE COMPLEX D, E, Zc, Zadj(0:3,0:500), Numer, Denom

C      File dZ.dat contains the output of the Cheng, Dodd, and Deeds code
      OPEN (2, FILE = 'dZ.dat', STATUS = 'NEW')
C      File Zadj.dat contains the impedance of the probe network
      (parallel cap, series R, parallel R, and Cheng, D & D impedance)
      OPEN (4, FILE = 'Zadj.dat', STATUS = 'NEW')
C      File contains the delta voltage across the probe network (time domain)
      OPEN (5, FILE = 'Vadj.dat', STATUS = 'NEW')

C      initialize constants
      Pi = 3.14159265359

C      initialize variables
      muo = Pi * 4E-7
      aStart = 0.
      aStop = 40.
      aStep = .1
      wStart = 6.28E3
      wStop = 1.57E6
      wStep = 6280.

      amp = 1.
      Icoil = .1

C      initialize coil paramaters
      N = 638
      Current = .1

      h1 = .000100
      h2 = .002640
      h = h2 - h1

      rin = .002795
      rout = .005335

```

```

rb = (rin + rout) / 2.

C   initialize sample parameters
C   Number of layers
    NumL = 5
C   Layer number which is corrosion
    CorLayer = 3
C   layers are numbered as in Cheng, Dodd, and Deeds, layer furthest
C   from the probe is layer(1)
C   conductivity of the layer(#)
    sigma(1) = 0.
    sigma(2) = 1.799E7
    sigma(3) = 1.799E7
    sigma(4) = 1.829E7
    sigma(5) = 0.
    sigma(6) = 0.
    sigma(7) = 0.
    sigma(8) = 0.
    sigma(9) = 0.
    sigma(10) = 0.
C   Permeability of the layer(#)
    mur(1) = 1.
    mur(2) = 1.
    mur(3) = 1.
    mur(4) = 1.
    mur(5) = 1.
    mur(6) = 0.
    mur(7) = 0.
    mur(8) = 0.
    mur(9) = 0.
    mur(10) = 0.
C   8mil corrosion, TOB
C   distance to layer(#)
    z(1) = -.0020650
    z(2) = -.0015570
    z(3) = -.0010236
    z(4) = -.000000
    z(5) = 0.
    z(6) = 0.
    z(7) = 0.
    z(8) = 0.
    z(9) = 0.
    z(10) = 0.

c   normalize variables
    rin = rin/rb
    rout = rout/rb
    h1 = h1/rb
    h2 = h2/rb
    h = h/rb
    z(1) = z(1)/rb
    z(2) = z(2)/rb
    z(3) = z(3)/rb
    z(4) = z(4)/rb
    z(5) = z(5)/rb
    z(6) = z(6)/rb
    z(7) = z(7)/rb
    z(8) = z(8)/rb
    z(9) = z(9)/rb
    z(10) = z(10)/rb

C   Compute Cheng, Dodd, and Deeds response
    K1 = (0., -1.) * Pi * (N**2) * muo * rb / ((h**2)*((rout+rin)**2))

```

```

mStop = INT((wStop - wStart)/wStep + .5)

Cpar = 9.08E-12
Rp = 1000.

DO count = 1, 2, 1

  DO m = 0, mStop, 1

    w = m * wStep + wStart

    K = K1 * w

    IF (count .EQ. 2) THEN
      sigma(CorLayer) = 0.
    END IF

    jStop = INT((aStop - aStart)/aStep + .5)

    DO j = 1, jStop, 1

      a = j * aStep

      DO n = 1, NumL, 1

        an(n) = SQRT(a**2 +
&          (0.,1.)*w*muo*mur(n)*sigma(n) * rb**2)

C      End the n loop

      END DO

      DO n = 1, (NumL - 1), 1
        Bn(n) = (mur(n+1) / mur(n) ) * (an(n)/an(n+1))

        H11(n) = .5*(1. + Bn(n))*EXP((an(n+1) - an(n)) *z(n))
        H12(n) = .5*(1. - Bn(n))*EXP((an(n+1) + an(n)) *z(n))
        H21(n) = .5*(1. - Bn(n))*EXP(-(an(n+1) + an(n))*z(n))
        H22(n) = .5*(1. + Bn(n))*EXP(-(an(n+1) - an(n))*z(n))

C      End the n loop
      END DO

      T11(1) = H11(1)
      T12(1) = H12(1)
      T21(1) = H21(1)
      T22(1) = H22(1)

      DO n = 1, (NumL - 2)

        T11(n+1) = H11(n+1) * T11(n) + H12(n+1) * T21(n)
        T12(n+1) = H11(n+1) * T12(n) + H12(n+1) * T22(n)
        T21(n+1) = H21(n+1) * T11(n) + H22(n+1) * T21(n)
        T22(n+1) = H21(n+1) * T12(n) + H22(n+1) * T22(n)

C      End the n loop
      END DO

      U11 = T11(NumL - 1)
      U12 = T12(NumL - 1)
      U21 = T21(NumL - 1)

```

```

U22 = T22(NumL - 1)
xStart = a*rin
xStop = a*rout
xStep = (xStop - xStart) / 400.
pStop = INT((xStop - xStart) / xStep + .5)
DO p = 0, pStop, 1
    xIntegration = xStart + p * (xStep)
    f(p) = xIntegration*bessj1(xIntegration)
C    End p (x) loop
    END DO

Sum1 = (0., 0.)
DO p = 0, (pStop - 1), 1
    Sum1 = Sum1 + ((f(p) + f(p+1))*xStep/2.)
C    End p loop
    END DO

I(j) = Sum1

c    -----Z computation from Cheng, Dodd, and Deeds-----
C1 = (U12/U22)*EXP(-2*a*h1)*(1-EXP(-a*h))-2
C(j) = -(I(j)**2 * (2*a*h + (1 - EXP(-a*h))*C1)/a**6)

c    -----
C    End j loop (alpha (a) integration loop)
    END DO

Sum2 = (0., 0.)
DO j = 1, (jStop - 1), 1
    Sum2 = ((C(j) + C(j+1)) * aStep / 2.) + Sum2
C    End j loop
    END DO

Z1(count, m) = K*Sum2
Rs = 49.
Zc = 1/((0., 1.) * w * Cpar)
Zadj(count, m) = 1/(1/Rp + 1/Zc + 1/(Z1(count,m) + Rs))
WRITE(4, 1000) w, Zadj(count,m)
1000  FORMAT(E20.10, E20.10, E20.10, E20.10)

freq = w / 2. / Pi
WRITE (*, 50) freq

```

```

50     FORMAT(E15.6)

C     End m loop (frequency loop)
      END DO

      END DO

c     Z1(1, x) is the impedance on null plate
c     Z1(2, x) is the impedance on a corroded sample
c     Z1(3, x) is the change in impedance Z1(1, x) - Z1(2, x)

DO m = 0, mStop, 1
    Z1(3,m) = Z1(1,m) - Z1(2,m)

    Zadj(3,m) = Zadj(1,m) - Zadj(2,m)

    w = m * wStep + wStart
    freq = w / 2. / Pi

    WRITE (*, 100) freq, Z1(3,m)

    WRITE (2, 100) freq, Z1(3,m)
100    FORMAT(E15.6, E15.6, E15.6, E15.6, E15.6)

      END DO

      NumPoints = mStop

      tStart = 0
      tStop = 500E-6
      tStep = 1E-6
      tCountStop = (tStop - tStart) / tStep + 1

      DO tCount = 0, tCountStop, 1

          time = tCount * tStep

          Sum = 0.

          DO m = 0, mStop, 1
              w = m * wStep + wStart

              Volt=(Icoil * REAL(Zadj(3,m)) * SIN(w*time) +
&                 Icoil * IMAG(Zadj(3,m)) * COS(w*time)) / w

              Sum = Sum + Volt

          END DO

          V(tCount) = -amp * Sum * wStep / Pi

          WRITE(5,900) time, V(tCount)

      END DO

900    FORMAT(E20.10, E20.10, E20.10)

      CLOSE(2)
      CLOSE(4)
      CLOSE(5)
      END

```



```

C      Bessel J1 function from Numerical Recipes in FORTRAN
      FUNCTION bessj1(x)
      REAL bessj1,x
      REAL ax,xx,zz
      DOUBLE PRECISION p1,p2,p3,p4,p5,q1,q2,q3,q4,q5,r1,r2,r3,r4,r5,r6,
      *s1,s2,s3,s4,s5,s6,y
      SAVE p1,p2,p3,p4,p5,q1,q2,q3,q4,q5,r1,r2,r3,r4,r5,r6,s1,s2,s3,s4,
      *s5,s6
      DATA r1,r2,r3,r4,r5,r6/72362614232.d0,-7895059235.d0,
      *242396853.1d0,-2972611.439d0,15704.48260d0,-30.16036606d0/,s1,s2,
      *s3,s4,s5,s6/144725228442.d0,2300535178.d0,18583304.74d0,
      *99447.43394d0,376.9991397d0,1.d0/
      DATA p1,p2,p3,p4,p5/1.d0,.183105d-2,-.3516396496d-4,
      *.2457520174d-5,-.240337019d-6/, q1,q2,q3,q4,q5/.04687499995d0,
      *-.2002690873d-3,.8449199096d-5,-.88228987d-6,.105787412d-6/
      if(abs(x).lt.8.) then
        y=x**2
        bessj1=x*(r1+y*(r2+y*(r3+y*(r4+y*(r5+y*r6))))/(s1+y*(s2+y*(s3+
      *y*(s4+y*(s5+y*s6))))
      else
        ax=abs(x)
        zz=8./ax
        y=zz**2
        xx=ax-2.356194491
        bessj1=sqrt(.636619772/ax)*(cos(xx)*(p1+y*(p2+y*(p3+y*(p4+y*
      *p5))))-zz*sin(xx)*(q1+y*(q2+y*(q3+y*(q4+y*q5)))))*sign(1.,x)
      endif
      return
      END
C (C) Copr. 1986-92 Numerical Recipes Software ~[]!-|2$.

```

**APPENDIX B. PUBLISHED PAPER: “LOW FREQUENCY, PULSED EDDY
CURRENTS FOR DEEP PENETRATION”**

Low Frequency, Pulsed Eddy Currents for Deep Penetration

W. W. Ward III and J. C. Moulder

Published in:

Review of Progress in QNDE, Vol. 17, eds by D. O. Thompson and D. E. Chimenti,
(Plenum Press, New York, 1998), in press.

LOW FREQUENCY, PULSED EDDY CURRENTS FOR DEEP PENETRATION

William W. Ward III and John C. Moulder
Center for NDE
Iowa State University
Ames, IA 50011

INTRODUCTION

Using eddy-currents to detect flaws buried deeply in a conducting material has always been a difficult problem. This is due in part to the fact that deep penetration requires low frequencies so that the skin depth is large enough for the eddy-currents to penetrate into the material the depth of the flaw. Also, low frequency eddy-current methods are beset with difficulties in probe design. In order to achieve the large inductance needed to operate at frequencies below 1 kHz, a large number of turns is needed, adding to the resistance of the coil and reducing the energy available to couple into the test piece. One solution is to use pulsed eddy-current methods, which operate efficiently and effectively with low inductance coils.

However, another limitation comes into play at low frequencies: coils respond to the time derivative of flux, $d\Phi/dt$, so that as the frequency is lowered their sensitivity is reduced. Pulsed eddy-current methods using pick up coils suffer from this limitation. Magnetic field sensors, on the other hand, respond to the total flux rather than its derivative, so they can be operated at very low frequencies without degrading performance. We explore the relative trade-off between using a coil or a magnetic field sensor in a pulsed eddy-current instrument. The magnetic field sensor used is one based on a giant magneto-resistive (GMR) sensing element. Relative abilities of the two systems to penetrate deeply into multiple layers of metal are measured and compared.

PEC SYSTEM

The pulsed eddy-current (PEC) system we used has been developed at the Center for NDE at Iowa State University as previously reported [1, 2]. The system is based on a portable personal computer with a custom made PEC card that contains the probe drive and signal amplifier electronics, an analog-to-digital converter expansion card, and a motor controller expansion board. The latter card is interfaced to a scanner equipped with stepper motors and is controlled by custom made software. The block diagram for this system is shown in Fig. 1.

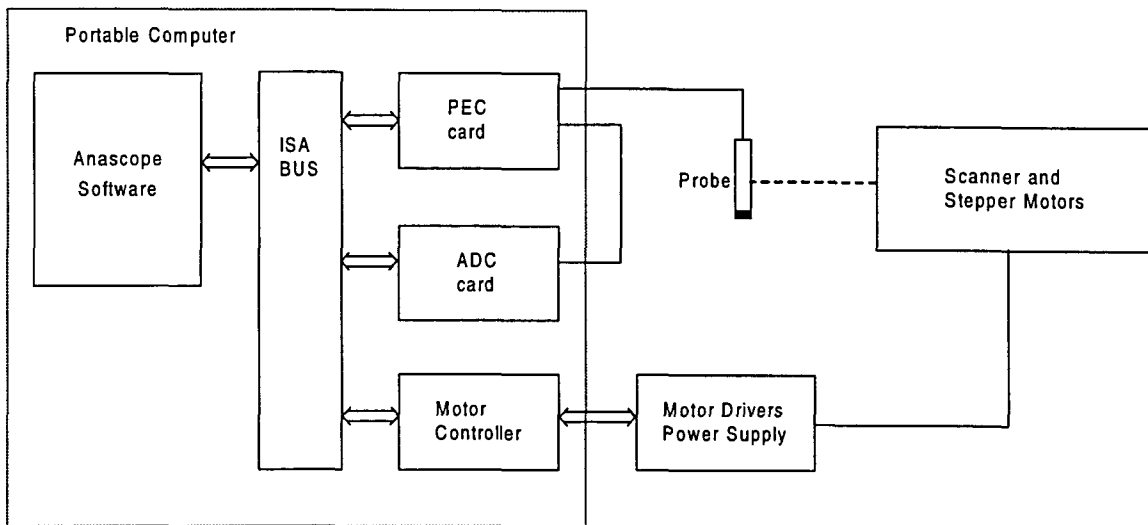


Figure 1. Block diagram for the pulsed eddy-current system.

The PEC system works as follows. The probe is driven with a rectangular voltage waveform operating with an on time of 10 ms and an off time of 40 ms. The response from the sensor on the rising edge of the drive voltage is recorded by the ADC at a location with no flaws as a null signal. The signal of interest is the change in the response of the sensor. As the probe is scanned, the signal recorded at each location is digitally subtracted from the null signal and displayed via the PC software. The amplitude of this difference signal contains information about the amount of metal loss and the time response contains information about the location (depth) of the corrosion.

The inherent advantage of the pulsed eddy-current system compared to a fixed-frequency or swept-frequency measurement stems from the fact that the measurement is a broad band measurement. One pulse contains information from a range of frequencies so the equivalent information of a swept-frequency measurement can be acquired on the order of milliseconds instead of minutes.

The GMR Sensor

The magnetic sensor used is a sensor based on the giant magnetoresistive effect and is shown schematically in Fig. 2. The sensor is made up of four GMR elements arranged in a resistance bridge configuration. Two of the elements are located between a pair of flux concentrators and their resistance changes in accordance with the applied magnetic field. These two elements are located on the opposing sides of the bridge. The other two elements are shielded from the magnetic field and are used to balance the bridge. This sensor has a directional sensitivity along the longitudinal axis of the 8-pin SOIC package and very little sensitivity to orthogonal fields. The bridge sensor is biased with a current source and the differential output of the bridge is amplified. The response of the sensor and electronics to an applied magnetic field is shown in Fig. 3.

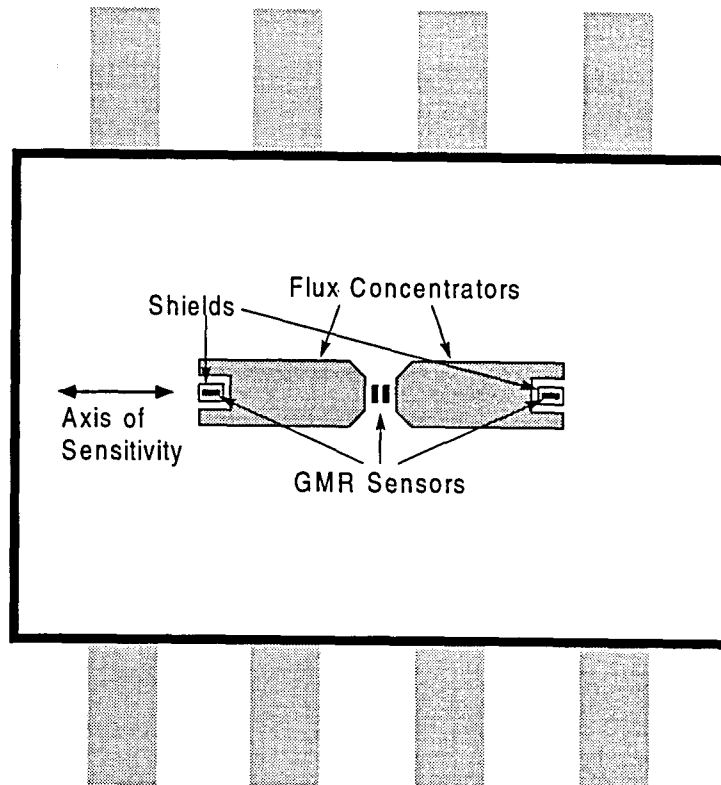


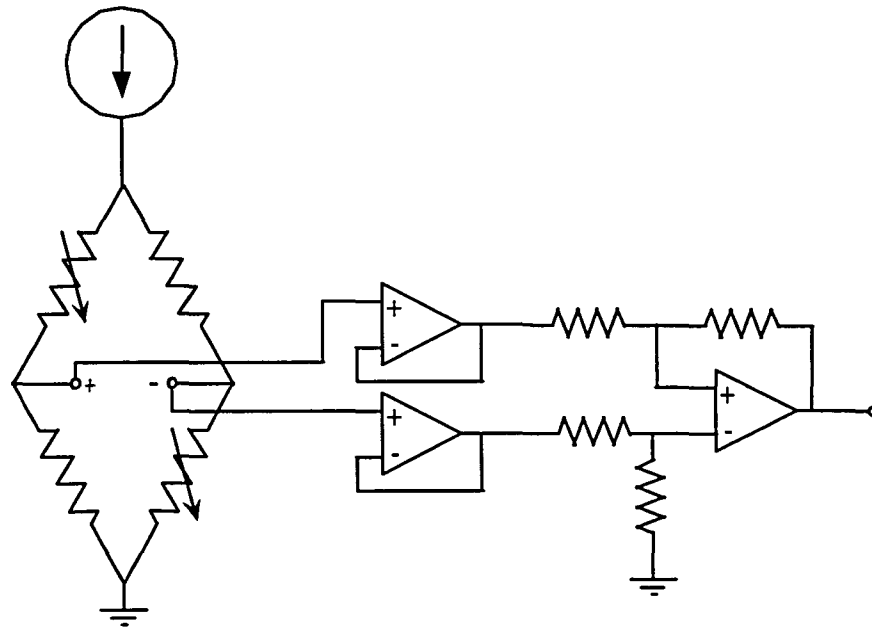
Figure 2. Schematic of the GMR sensor.

Probe Design

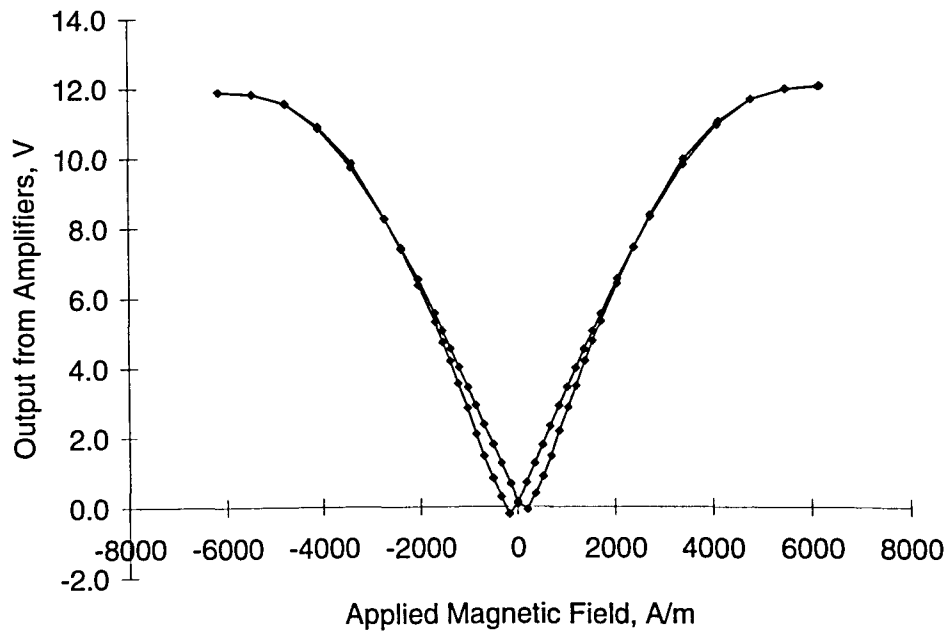
A significant advantage of the pulsed eddy-current system for deep penetration when compared to the traditional fixed-frequency instrument is that the probes are easier to build and design. For a continuous wave system operating at 100 Hz (which would be required to reach depths of 6 to 12 mm), an impedance of approximately 50 ohms would be required to operate with traditional eddy-current instruments. This would translate to an inductance of 80 mH if the inductor were lossless. However, in a practical design the resistance of the wire would dominate the impedance of the coil. For a coil of similar dimensions to the one used with the pulsed eddy-current system with a total impedance of 50 ohms, 1750 turns would be required. The inductance would be 30 mH and the DC resistance of the wire would be 34 ohms out of the total of 50 ohms. This makes it difficult to fabricate a coil to operate at these depths with traditional eddy-current instruments. Pulsed eddy-current systems do not have this impedance limitation. The probe used for the pulsed eddy-current system is shown in Fig. 4.

THEORY

When comparing the fall off of the signal with depth for a pulsed eddy-current system, it is not obvious how the signal will decrease. Because of this, simulations were performed for the magnetic sensor and the coil sensor configurations to determine the fall off of the two sensors. The simulation for the coil sensor is based on the Cheng, Dodd, and Deeds formulation [3] applied to the transient pulsed eddy-current system by Rose, Uzal,



(A)



(B)

Figure 3. (A) The circuitry used to drive the bridge sensor and sense the output signal. (B) The output response of the sensor due to magnetic stimulus.

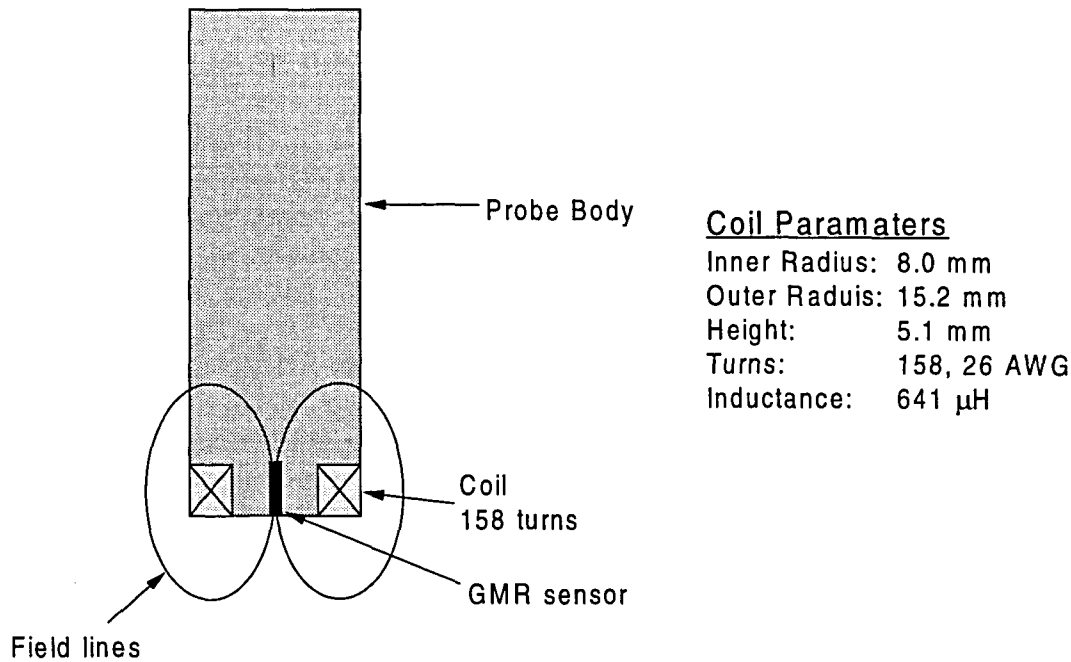


Figure 4. Pulsed eddy-current probe design.

and Moulder [4]. The magnetic sensor simulation is based on the formulation by Bowler and Harrison [5] and Johnson [6]. The software for the magnetic sensor simulation was written by Bowler. The simulation results are for a panel of 2024 Al with 10% metal loss. To allow for comparison between the magnetic signals and the current signal from the coil sensor, the signals are normalized to $\Delta H/H$ and $\Delta I/I$.

The normalized peaks of these signals versus thickness of the sample, hence depth of penetration, are plotted in Fig. 5. Looking at Fig. 5 (B) it can be seen that the signal from the magnetic sensor is three times as strong as the coil sensor for a 4 mm thick sample and increases to ten times the strength for a 15 mm thick sample.

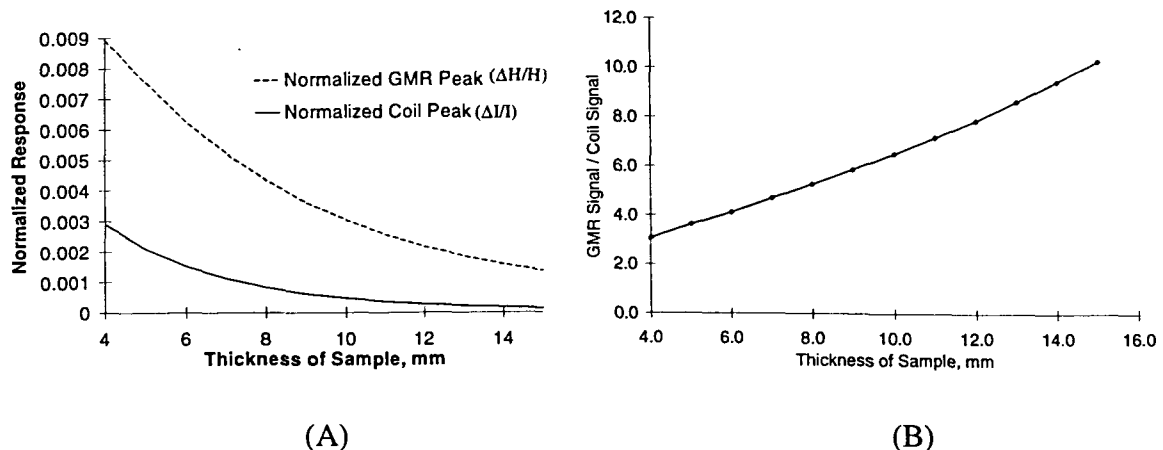


Figure 5. Theoretical predictions of the coil sensor and GMR sensor for detecting 10% corrosion on the bottom of a 2024 Al panel. (A) The peak of the normalized signal vs. thickness of sample. (B) Comparison of the signal strength between the two sensors.

EXPERIMENTAL RESULTS

The probe was tested using it in both the absolute coil sensor mode, where the same coil is used as both drive and receive coil, and also in the magnetic sensor mode, where the eddy-currents are induced by the coil and the change in the magnetic field incident on the GMR sensor is the received signal. These two configurations were used to detect simulated corrosion (flat bottom holes) on the bottom of 6.3 mm thick and 12.7 mm thick 2024 Al panels.

For the 6.3 mm thick panel, both probes could detect the entire range of simulated corrosion present in the sample, ranging from 5% to 50% of the total thickness. The signals are shown in Fig. 6. The normalized signal from the magnetic probe for 10% corrosion is 3.55×10^{-3} for the magnetic sensor and 1.23×10^{-3} for the coil sensor. Thus, the signal strength for the magnetic sensor is 2.9 times the strength of the coil sensor. This is in reasonable agreement with the predicted ratio of 4.1 in Fig. 5 (B).

Using the GMR sensor mode, the probe was fixed in the scanning fixture and the sample was scanned. The result is shown in Fig. 7, illustrating the ability of the magnetic sensor-based system to image areas of corrosion using the same software developed for the coil-based system.

Measurements were also taken on a sample of 2024 Al 12.7 mm thick with simulated corrosion ranging from 2.5% to 25% on the bottom of the panel. As shown in Fig. 8, both sensors were able to detect the 25%, 15%, and 10% corrosion. However, the GMR sensor was more sensitive and was able to detect levels of corrosion down to 2.5% as well.

As expected, the signal from the GMR sensor was stronger than the coil sensor. For 10% corrosion, the normalized peak signal level from the GMR sensor was 1.9×10^{-3} while the normalized peak signal level from the coil sensor was 0.257×10^{-3} . Thus the signal from the GMR sensor is 7.4 times the strength of the coil sensor. This is in good agreement with the predicted ratio of 8.4 in Fig. 5 (B).

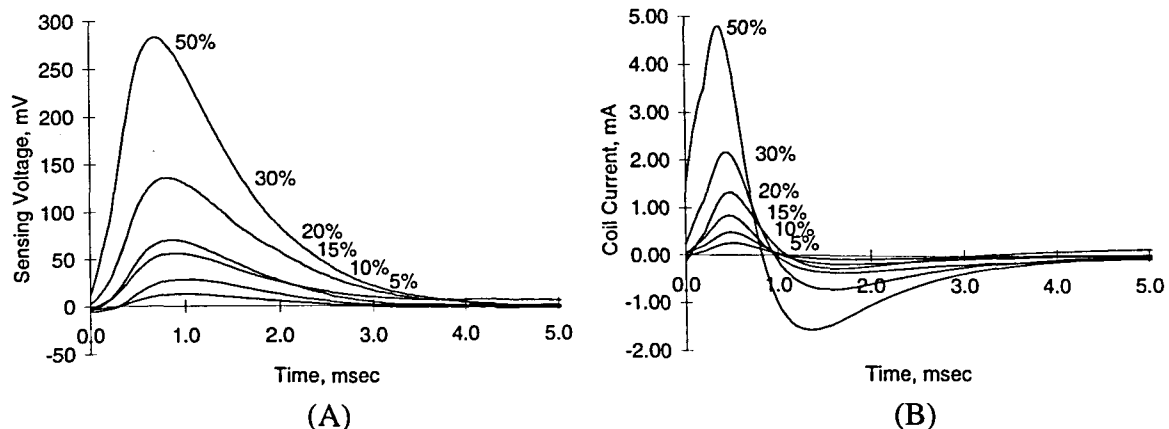


Figure 6. Signals for simulated corrosion on the bottom of a 6.3 mm panel of 2024 Al for the GMR sensor (A) and the coil sensor (B).

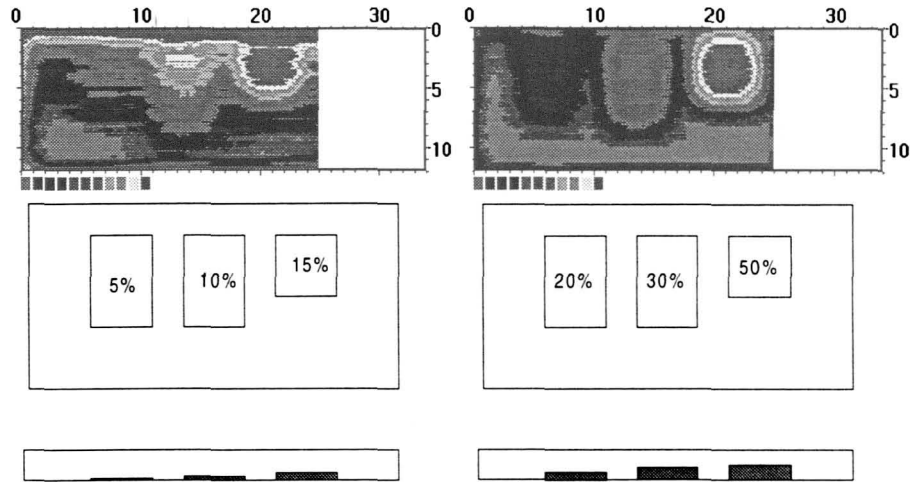


Figure 7. Scanned images using the GMR probe to detect simulated corrosion on the bottom of a 6.3 mm thick panel of 2024 Al.

DISCUSSION AND SUMMARY

The ability of a giant magnetoresistive sensor to detect corrosion through thick plates of aluminum was investigated. First, it was determined by theoretical calculations that the signal from the GMR sensor is stronger than the coil sensor at deep penetration levels. Since this is true in the continuous wave approach and pulsed eddy-currents are a measurement containing a range of frequencies, the same general trend was expected when the sensor was used in a pulsed eddy current instrument.

Given the stronger signal, it was expected that the GMR sensor would be significantly better at detecting deeply buried corrosion. This was verified experimentally by looking at corrosion on the bottom of 6.3 mm thick and 12.7 mm thick 2024 Al plates. For the case of corrosion on the bottom of the half-inch thick plates, the GMR sensor performed markedly better. Its signal was approximately 8 times the strength of the coil sensor and it

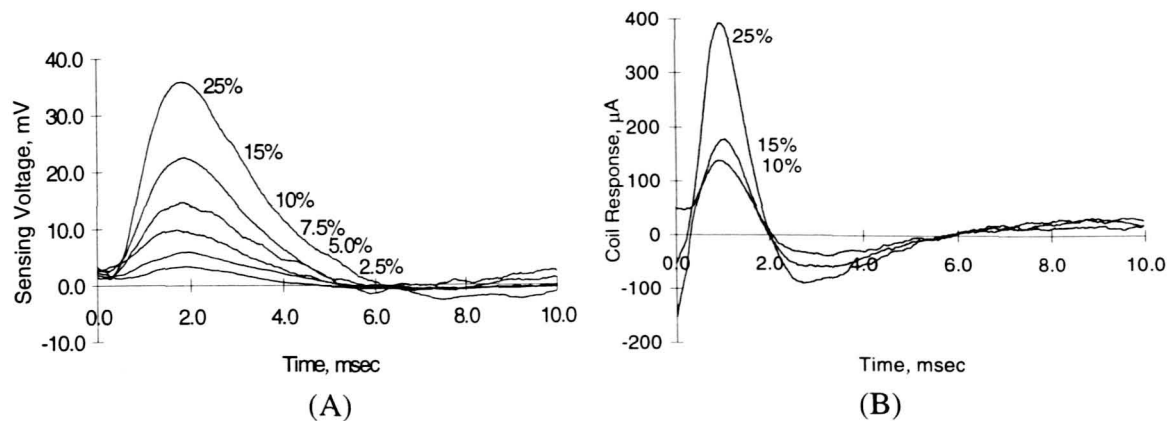


Figure 8. Signals for simulated corrosion on the bottom of a 12.7 mm panel of 2024 Al for the GMR sensor (A) and the coil sensor (B).

was able to detect corrosion down to 2.5%. The coil sensor was only able to detect simulated corrosion down to 10% metal loss.

These results demonstrate that for deep penetration using pulsed eddy currents, the magnetic sensor is preferred over a coil sensor. It is clear that the giant magnetoresistive sensor performed well as a magnetic sensor for pulsed eddy current detection of corrosion, owing to its sensitivity, ease of use, and compactness.

ACKNOWLEDGMENT

This work is supported by the FAA Center for Aviation Systems Reliability program under Federal Aviation Administration Grant No. 95G-032. We are grateful to Dr. Marcus Johnson and Prof. John Bowler for their assistance in calculating magnetic field strengths for this article.

REFERENCES

1. J. C. Moulder, M. W. Kubovich, E. Uzal, and J. H. Rose, "Pulsed eddy-current measurements of corrosion-induced metal loss: theory and experiment," *Review of Progress in Quantitative NDE*, Vol. 14, edited by D. O. Thompson and D. E. Chimenti, (Plenum Press, New York, 1995) pp. 2065-2072.
2. J. C. Moulder, J. A. Bieber, W. Ward III, and J. H. Rose, "Scanned pulsed-eddy-current instrument for non-destructive inspection of aging aircraft," in *Nondestructive Evaluation of Aging Aircraft, Airports, and Aerospace Hardware*, edited by R. D. Rempt and A. L. Broz, SPIE Vol. 2945, (SPIE, Bellingham, 1996) pp. 2-13.
3. C. C. Cheng, C. V. Dodd, and W. E. Deeds, *Int. J. Nondestr. Test* 3, 109 (1971).
4. J. H. Rose, E. Uzal, and J. C. Moulder, "Pulsed eddy-current characterization of corrosion in aircraft lap splices: Quantitative modeling," in *Superconductive Devices and Circuits*, edited by Robert A. Buhman; John T. Clarke; Ken Daly; Roger H. Koch; Jerome A. Luine; and Randy W. Simon; SPIE Vol. 2160, (SPIE, Bellingham, 1994) pp. 164-176.
5. J. R. Bowler and D. J. Harrison, "Measurement and calculation of transient eddy-currents in layered structures," *Review of Progress in Quantitative NDE*, Vol. 12, edited by D. O. Thompson and D. E. Chimenti, (Plenum Press, New York, 1993) pp. 2003 - 2010.
6. M. J. Johnson, "The use of transient eddy-currents for imaging 3-D metallic structures," Ph.D. Dissertation, University of Surrey, 1994, pp. 15-20.

BIBLIOGRAPHY

1. S. Mitra, P. S. Urali, E. Uzal, J. H. Rose, and J. C. Moulder, "Eddy-current measurements of corrosion-related thinning in aluminum lap splices," in *Review of Progress in QNDE*, Vol. 12B, edited by D. O. Thompson and D. E. Chimenti, (Plenum Press, New York, 1993).
2. J. C. Moulder, J. A. Bieber, W. W. Ward III, and J. H. Rose, "Scanned pulsed eddy-current instrument for non-destructive inspection of aging aircraft," in *Proceedings of the SPIE Conference on Nondestructive Evaluation of Aging Aircraft, Airports, and Aerospace Hardware, Volume 2945*, edited by Raymond D. Rempt and Alfred L. Broz. SPIE Vol 2945, (SPIE, Bellingham, 1996) pp. 2-13.
3. W. W. Ward III and J. C. Moulder, "Low Frequency, Pulsed Eddy Currents for Deep Penetration," *Review of Progress in QNDE*, Vol. 17, edited by D. O. Thompson and D. E. Chimenti, (Plenum Press, New York, 1998), in press.
4. J. A. Bieber, C. Tai, and J. C. Moulder, "Quantitative Assessment of Corrosion in Aircraft Structures Using Scanning Pulsed Eddy Current," *Review of Progress in QNDE*, Vol. 17, edited by D. O. Thompson and D. E. Chimenti, (Plenum Press, New York, 1998), in press.
5. C. Tai, J. H. Rose, and J. C. Moulder, "Thickness and Conductivity of Metallic Layers from Pulsed Eddy-Current Measurements," *Rev. Sci. Instrum.* 67 (11), November 1996, (American Institute of Physics, 1996), pp. 3965-3972.
6. J. A. Bieber, S. K. Shaligram, J. H. Rose, and J. C. Moulder, "Time-Gating of Pulsed Eddy Current Signals for Defect Characterization and Discrimination in Aircraft Lap-Joints," *Review of Progress in QNDE*, Vol. 16B, edited by D. O. Thompson and D. E. Chimenti, (Plenum Press, New York, 1997), pp. 1915-1921.
7. T. C. Patton and D. K. Hsu, "Field Demonstrations of the Dripless Bubbler Ultrasonic Scanner," *Review of Progress in QNDE*, Vol. 14B, edited by D. O. Thompson and D. E. Chimenti, (Plenum Press, New York, 1995), pp 2269-2276.
8. J. C. Moulder, M. W. Kubovich, E. Uzal, and J. H. Rose, "Pulsed eddy-current measurements of corrosion-induced metal loss: Theory and experiment," *Review of Progress in QNDE*, Vol. 14B, edited by D. O. Thompson and D. E. Chimenti, (Plenum Press, New York, 1995), pp. 2065-2072.
9. S. K. Shaligram, "Development of a pulsed eddy current instrument for corrosion detection," Master's Thesis, Iowa State University, 1996.
10. C.C. Cheng, C. V. Dodd, and W. E. Deeds, *Int. J. Nondestr. Test* 3, 109 (1971).

11. J. H. Rose, E. Uzal, and J. C. Moulder, "Pulsed eddy-current characterization of corrosion in lap splices: Quantitative modeling," in *Superconductive Devices and Circuits*, edited by Robert A. Buhrman; John T. Clarke; Ken Daly; Roger H. Koch; Jerome A Luine; and Randy W. Simon. SPIE Vol. 2160, (SPIE, Bellingham, 1994) pp. 164-176.
12. C. H. Smith and R. W. Schneider, "The growing role of solid-state magnetic sensing," Nonvolatile Electronics, Inc., Eden Prairie, MN, 1997.
13. J. Daughton, J. Brown, R. Beech, A. Pohm, and B. Kude, "Magnetic field sensors using GMR multilayer," *IEEE Transactions on Magnetics*, Vol. 30, No. 6, (1994), pp. 4608-4610.
14. J. R. Bowler and D. J. Harrison, "Measurement and calculation of transient eddy-currents in layered structures," *Review of Progress in Quantitative NDE*, Vol. 12, edited by D. O. Thompson and D. E. Chimenti, (Plenum Press, New York, 1993), pp. 2003 - 2010.
15. M. J. Johnson, "The use of transient eddy-currents for imaging 3-D metallic structures," Master's Thesis, University of Surrey, 1994, pp. 15-20.
16. D. L. Waidelich, "Pulsed Eddy-Current Testing of Steel Sheets," *Eddy Current Characterization of Materials and Structures, ASTM STP 722*. George Birnbaum and George Free, Eds., American Society for Testing and Materials, 1981, pp. 367-373.
17. W. Podney and J. Moulder, "Electromagnetic Microscope for Deep, Pulsed, Eddy Current Inspections," *Review of Progress in QNDE*, Vol. 16A, edited by D. O. Thompson and D. E. Chimenti, (Plenum Press, New York, 1997), pp 1037-1044.
18. W. F. Arvin, "Magnetoresistive Eddy-Current Sensor for Detecting Deeply Buried Flaws," *Review of Progress in QNDE*, Vol. 15A, edited by D. O. Thompson and D. E. Chimenti, (Plenum Press, New York, 1996), pp 1145-1150.